Precipitation Climatology in an Ensemble of CORDEX-Africa Regional Climate Simulations

GRIGORY NIKULIN,[a] COLIN JONES,[a] FILIPPO GIORGI,[b] GHASSEM ASRAR,[c] MATTHIAS BÜCHNER,[d] RUTH CEREZO-MOTA,[e] OLE BØSSING CHRISTENSEN,[f] MICHEL DÉQUÉ,[g] JESUS FERNANDEZ,[h] ANDREAS HÄNSLER,[i] ERIK VAN MEIJGAARD,[j] PATRICK SAMUELSSON,[a] MOUHAMADOU BAMBA SYLLA,[b] AND LAXMI SUSHAMA[k]

[a] *Rossby Centre, Swedish Meteorological and Hydrological Institute, Norrköping, Sweden*
[b] *Abdus Salam International Centre for Theoretical Physics, Trieste, Italy*
[c] *World Climate Research Programme, Geneva, Switzerland*
[d] *Potsdam Institute for Climate Impact Research, Potsdam, Germany*
[e] *University of Cape Town, Cape Town, South Africa*
[f] *Danmarks Meteorologiske Institut, Copenhagen, Danmark*
[g] *Centre National de Recherches Météorologiques, Météo-France, Toulouse, France*
[h] *Universidad de Cantabria, Santander, Spain*
[i] *Climate Service Center, Helmholtz-Zentrum Geesthacht, Hamburg, Germany*
[j] *Koninklijk Nederlands Meteorologisch Instituut, De Bilt, Netherlands*
[k] *Université du Québec à Montréal, Montréal, Quebec, Canada*

(Manuscript received 4 July 2011, in final form 2 December 2011)

ABSTRACT

An ensemble of regional climate simulations is analyzed to evaluate the ability of 10 regional climate models (RCMs) and their ensemble average to simulate precipitation over Africa. All RCMs use a similar domain and spatial resolution of ~50 km and are driven by the ECMWF Interim Re-Analysis (ERA-Interim) (1989–2008). They constitute the first set of simulations in the Coordinated Regional Downscaling Experiment in Africa (CORDEX-Africa) project. Simulated precipitation is evaluated at a range of time scales, including seasonal means, and annual and diurnal cycles, against a number of detailed observational datasets. All RCMs simulate the seasonal mean and annual cycle quite accurately, although individual models can exhibit significant biases in some subregions and seasons. The multimodel average generally outperforms any individual simulation, showing biases of similar magnitude to differences across a number of observational datasets. Moreover, many of the RCMs significantly improve the precipitation climate compared to that from their boundary condition dataset, that is, ERA-Interim. A common problem in the majority of the RCMs is that precipitation is triggered too early during the diurnal cycle, although a small subset of models does have a reasonable representation of the phase of the diurnal cycle. The systematic bias in the diurnal cycle is not improved when the ensemble mean is considered. Based on this performance analysis, it is assessed that the present set of RCMs can be used to provide useful information on climate projections over Africa.

1. Introduction

There is a growing interest from a wide range of decision makers for climate change information on regional to local scales and at high spatial resolution. The primary tool for providing future climate projections is atmosphere–ocean general circulation models (AOGCMs), which simulate climate changes under a range of future greenhouse gas emission scenarios. Present-day AOGCMs have spatial resolution of order 100–250 km. Despite rapid advances in high-performance computing, computational demands still limit the use of high-resolution (50 km or better) AOGCMs for multicentury simulations, while a few AOGCM simulations have been run for short time slice periods at such high resolutions (e.g., Oouchi et al. 2006). Because of the dual constraint of providing an ensemble of projections over long periods, AOGCMs cannot fulfill the requirements of high spatial detail required by many users and are

Corresponding author address: Grigory Nikulin, Rossby Centre, Swedish Meteorological and Hydrological Institute, Folkborgsvägen 1, S-60176 Norrköping, Sweden.
E-mail: grigory.nikulin@smhi.se

DOI: 10.1175/JCLI-D-11-00375.1

therefore generally supplemented with statistical or dynamical downscaling to produce future climate projections at regional scales.

Over the past decade, several international projects have applied regional climate models (RCMs) to generate high-resolution, multimodel ensembles of future climate projections by downscaling output from AOGCMs. These include the Prediction of Regional Scenarios and Uncertainities for Defining European Climate Change Risks and Effects (PRUDENCE) (Christensen et al. 2007) and ENSEMBLE-Based Predictions of Climate Changes and their Impacts (ENSEMBLES) (van der Linden and Mitchell 2009) for Europe; the North American Regional Climate Change Assessment Program (NARCCAP) (Mearns et al. 2009) for North America; Europe–South America Network for Climate Change Assessment and Impact Studies in La Plata Basin (CLARIS-LPB) (Menéndez et al. 2010) over South America and ENSEMBLES–African Monsoon Multidisciplinary Analyses (AMMA) (van der Linden and Mitchell 2009) for West Africa. Each of these projects has made significant contributions to downscaling efforts over their specific region, but there has been very limited international coordination of such projects and therefore limited transfer of knowledge between projects and regions. A new initiative—the Coordinated Regional climate Downscaling Experiment (CORDEX) (Giorgi et al. 2009; Jones et al. 2011), sponsored by the World Climate Research Programme—aims to fill this gap by coordinating international efforts in regional climate downscaling. CORDEX is organized in a similar manner to the Coupled Model Intercomparison Project phase 5 (CMIP5) for global model simulations, with predefined regions, grids, experiment protocols, output variables, and output format facilitating easier analysis of possible future regional climate changes, not only by the scientific community, but also by end-user communities at regional and local levels.

Twelve regions, covering the majority of the populated land areas worldwide, plus both the Arctic and Antarctic, have been defined within CORDEX. An initial focus in CORDEX will be on Africa, which is particularly vulnerable to climate change and has a low adaptive capacity. For example, water supply and food security are of critical importance in Africa; we therefore emphasize the quality of RCM-simulated precipitation as a major driver for both sectors over Africa. Many studies have examined the performance of a single RCM, driven by the reanalysis, in simulating precipitation over different parts of Africa: the fifth-generation Pennsylvania State University–National Center for Atmospheric Research Mesoscale Model (MM5) (Tadross et al. 2006), the Weather Research and Forecasting model (WRF) (Patricola and Cook 2010), the Regional Climate Model, version 3 (RegCM3) (Afiesimama et al. 2006; Anyah and Semazzi 2007; Pal et al. 2007; Sylla et al. 2009, 2010), and the Regional Model (REMO) (Paeth et al. 2005; Haensler et al. 2010). However, few studies have focused on simulated precipitation from an ensemble of different RCMs, as, for example, Druyan et al. (2010) and Paeth et al. (2011) have recently done for West Africa. All studies indicate that RCMs are able to capture the main climatological features of precipitation but with quite different levels of accuracy depending on the model, region, and season, with the multimodel average generally outperforming individual RCMs (Paeth et al. 2011).

In this study we present the first results of the CORDEX-Africa project by evaluating an ensemble of 10 RCM simulations, covering the entire African continent and driven by the European Centre for Medium-Range Weather Forecasts (ECMWF) Interim Re-Analysis [ERA-Interim (ERAINT)]. The performance of the individual RCMs and their ensemble average is documented in detail at a range of time scales. We begin by evaluating simulated seasonal mean climatologies, followed by a more detailed analysis of seasonal precipitation associated with the West African monsoon (WAM). We then evaluate the simulated annual and diurnal cycles of precipitation over a number of different African regions characterized by different climate regimes. In next section we first present a brief description of the data, models, and methods.

2. Data and method

a. Model simulations

An ensemble of 10 different RCMs is utilized for this study. A full list of the participating RCMs and details of their dynamics and physical parameterizations is presented in Table 1. All simulations are performed at ~50-km resolution over the same CORDEX Africa domain (Fig. 1) and use ERA-Interim (1989–2008) as lateral boundary conditions. No nudging toward ERAINT was applied in any of the RCMs within the model domain. One model—Action de Recherche Petite Echelle Grande Echelle (ARPEGE)—is a global variable resolution model. ARPEGE uses a high-resolution region, within its continuous global domain, coincident in resolution and geographic area with the RCMs. Within this region no nudging toward ERAINT was applied; however, outside the high-resolution region, nudging was applied to keep the inflow into the high-resolution region comparable to the boundary data specified for the other RCMs. With respect to spectral nudging of an RCM solution toward the driving data at large wavelengths

(von Storch et al. 2000), this technique is well established for midlatitude regions, with some theoretical understanding of which wavelengths should be nudged and at what altitudes (Alexandru et al. 2009). This is not the case in the tropics, and it may be more difficult to formulate given the stronger role of surface forcing and multiscale convection in driving large-scale circulations. We therefore chose to preclude spectral nudging from the experimental design, pending further work in this area. The ERAINT sea surface temperature (SST) is used as the ocean boundary conditions in 8 of the 10 RCMs, while RegCM uses the National Oceanic and Atmospheric Administration (NOAA) weekly optimum interpolation SST and the Canadian Regional Climate Model (CRCM) uses the Atmospheric Model Intercomparison Project, phase 2 (AMIP2) SST. For analysis we collect 3-hourly total precipitation, averaged for 0000–0300, 0300–0600, . . . 2100–0000 universal time (UTC), which is then also averaged into daily and monthly means.

b. Observations and reanalysis

One of the main problems in evaluating RCM simulations over Africa is a lack of high-quality observation datasets at suitable temporal and spatial resolution. In recent decades satellite measurements have partly improved the situation, and here we use two satellite-based precipitation products with 0.25° spatial and 3-hourly temporal resolution: the Tropical Rainfall Measuring Mission (TRMM 3B42 version 6, 1998–2010; Huffman et al. 2007) and the Climate Prediction Center morphing technique (CMORPH, 2003–10; Joyce et al. 2004). CMORPH represents 3-hourly precipitation estimates for the same time intervals as the RCMs, while TRMM precipitation averages are shifted by one and one-half hours, representing approximately the 22:30–01:30, 01:30–04:30, . . . 19:30–22:30 UTC intervals. Several studies report that the timing of peak rainfall during the day in satellite products, including infrared (IR) sensor data (both TRMM-3B42 and CMORPH in our case), may be delayed by ~3 h compared to radar/microwave satellite precipitation estimates. This is because IR sensors do not directly detect rain, but rather brightness temperature at the top of convective clouds (Kikuchi and Wang 2008; Yamamoto et al. 2008). However, Pinker et al. (2006) show that for a site in Nigeria, CMORPH is exactly in phase with ground-based observations. To resolve this issue, we have additionally analyzed the TRMM-3G68 precipitation, which includes precipitation rates from a precipitation radar, microwave imager, and their combination (ftp://trmmopen.gsfc.nasa.gov/pub). In contrast to some earlier studies, we find no significant difference in the daily phase of precipitation over Africa between the two TRMM datasets and therefore use only the CMORPH and TRMM-3B42 as primary observations for analysis of the diurnal cycle.

To estimate observational uncertainties, we include in our analysis four gridded observational datasets with coarser temporal and spatial resolution than TRMM and CMORPH. The Global Precipitation Climatology Project (GPCP, version 1.1, 1998–2010) satellite–gauge combination covers the entire African domain with a 1° spatial and daily temporal resolution (Huffman et al. 2001). Three gauge-based datasets are available at 0.5° spatial and monthly temporal resolution: the University of Delaware (UDEL version 2.01, 1901–2008; Legates and Willmott 1990), the Climatic Research Unit at the University of East Anglia (CRU version 3.1, 1901–2009; Mitchell and Jones 2005), and the Global Precipitation Climatology Centre (GPCC version 5, 1901–2009; Rudolf et al. 2010). Each dataset covers different periods. We use three analysis periods for different aspects of the African precipitation climatology and try to include as many observational datasets as possible in each analysis. The periods are 1990–2008 (1989 is spinup) for interannual variability analysis, 1998–2008 (limited by TRMM and GPCP) for observational uncertainty/seasonal mean/annual cycle, and 2003–08 (limited by CMORPH) for the diurnal cycle. Although some of these periods are rather short, we find that the obtained results are insensitive to the period chosen, for example, longer periods—1990–2008 instead of 1998–2008 for the seasonal mean (without GPCP and TRMM) or 1998–2008 instead of 2003–08 for the diurnal cycle (without CMORPH)—do not change the results.

Precipitation from ERAINT is also compared to the RCM results and observations. We note that ERAINT precipitation is a forecast product, and there are several ways to derive ERAINT precipitation (e.g., different spinup, base time, and forecast steps) that can lead to different precipitation estimates (Dee et al. 2011). Two methods (with and without spinup) to derive the 3-hourly and daily precipitation have been tested, and we have found only minor differences in the results obtained with these two methods. Given the uncertainty as to which method is most appropriate, we derive ERAINT precipitation by the simplest method, without spinup: 3-hourly precipitation uses the base times 0000 and 1200 and forecast steps 3, 6, 9, and 12 h, while daily precipitation uses base times 0000 and 1200 and forecast steps of 12 h. Monthly means are calculated by averaging the daily means.

c. Methods

Most RCM simulations are performed on the same rotated grid with 0.44° horizontal resolution. This is used

TABLE 1. List of RCMs and their details. SUBEX = subgrid explicit moisture scheme; ISBA = Interactions between Soil, Biosphere, and Atmosphere; WSM5 = WRF single-moment 5-class scheme; BATS1E = Biosphere–Atmosphere Transfer Scheme version 1e; TERRA-ML = TerraLib Modeling Language; TESSEL = Tiled ECMWF Scheme for Surface Exchanges over Land; MOSES2 = Met Office Surface Exchange Scheme version 2; CLASS 3.5 = Canadian Land Surface Scheme version 3.5.

	CNRM ARPEGE5.1	DMI HIRHAM5	ICTP RegCM3	CLMcom CCLM4.8
Institute	Centre National de Recherches Météorologiques, France	Danmarks Meteorologiske Institut, Denmark	Abdus Salam International Centre for Theoretical Physics, Italy	Climate Limited-Area Modelling Community (www.clm-community.eu)
Short name	ARPEGE	HIRHAM	RegCM3	CCLM
Projection resolution	Polar, stretching factor 2 (TL179)	Rotated pole 0.44°	Mercator 50 km	Rotated pole 0.44°
Vertical coordinate/levels	Hybrid/31	Hybrid/31	Sigma/18	Terrain following/35
Advection	Semi-Lagrangian	Semi-Lagrangian	Eulerian	Fifth-order upwind; Baldauf (2008)
Time step (s)	1200	600	100	240
Convective scheme	Bougeault (1985)	Tiedtke (1989)	Grell (1993) Fritsch and Chappell (1980)	Tiedtke (1989)
Radiation scheme	Morcrette (1990)	Fouquart and Bonnel (1980); Mlawer et al. (1997)	Kiehl et al. (1996)	Ritter and Geleyn (1992)
Turbulence vertical diffusion	Mellor and Yamada (1982)	Louis (1979)	Holtslag et al. (1990)	Herzog et al. (2002); Buzzi et al. (2011)
Cloud microphysics scheme	Ricard and Royer (1993)	Tiedtke (1989); Tompkins (2002)	SUBEX; Pal et al. (2000)	Doms et al. (2011); Baldauf and Schulz (2004)
Land surface scheme	ISBA; Douville et al. (2000)	Schulz et al. (1998); Hagemann (2002)	BATS1E; Dickinson et al. (1993)	TERRA-ML; Doms et al. (2011)
Latest reference and comments	Déqué (2010)	Christensen et al. (2006)	Pal et al. (2007)	Rockel et al. (2008); Baldauf et al. (2011)

as a reference grid, and all datasets on other grids are remapped to this reference grid. The TRMM and CMORPH datasets are aggregated from the native 0.25° grid onto the reference grid by a first-order conservative remapping (Jones 1999), while all other datasets, with similar or coarser resolution than 0.44°, are remapped through bilinear interpolation.

The climatological annual cycle, calculated from daily data, has a significant amount of high-frequency noise due to the relatively short sampling period and large day-to-day precipitation variability. To highlight the slow-varying annual cycle, we apply a finite impulse response filter (Smith 2002) with a 50-day cutoff period, which is approximately equivalent to the widely used 30-day moving average but with better frequency response. The filter length is chosen equal to the cutoff period in days.

The climatological diurnal cycle is estimated from 3-hourly precipitation. A common way to determine the phase and amplitude of the diurnal cycle based on discrete data is to approximate it by the diurnal and semi-diurnal (Fourier) harmonics (Dai et al. 2007; Jeong et al. 2011). As the harmonic analysis is not the only available method and may be not the best approach, especially if the diurnal cycle is nonharmonic (Yang and Smith 2006), we also fit a cubic spline to the 3-hourly precipitation. Although the results based on the harmonic and cubic spline approaches are quite similar, on average the cubic spline gives a better description of the diurnal cycle, capturing smaller-scale features. We have tested several precipitation thresholds in calculating the diurnal cycle, by including in our analysis only days with total daily accumulations greater than 1, 2, and 3 mm day^{-1}. Use of these different thresholds results in different amplitudes of the diurnal cycle but does not affect the phase. We therefore decided to impose an accumulation threshold of 1 mm day^{-1} to determine which days to be included in our calculation of the diurnal cycle to exclude nonrepresentative dry days.

3. Observational uncertainties

We first evaluate the spread among the different observational datasets over Africa to get an estimate of the observational accuracy available for model evaluation. All the gridded products agree quite well with respect to large-scale precipitation patterns, but significant deviations can occur locally (Gruber et al. 2000; Fekete

TABLE 1. (*Extended*)

KNMI RACMO2.2b	MPI REMO	SMHI RCA35	UCT PRECIS	UC WRF3.1.1	UQAM CRCM5
Koninklijk Nederlands Meteorologisch Instituut, Netherlands	Max Planck Institute, Germany	Sveriges Meteorologiska och Hydrologiska Institut, Sweden	University of Cape Town, South Africa	Universidad de Cantabria, Spain	Université du Québec à Montréal, Canada
RACMO	REMO	RCA	PRECIS	WRF	CRCM
Rotated pole 0.44°	Rotated pole 0.44°	Rotated pole 0.44°	Rotated pole 0.44°	Mercator 50 km	Rotated pole 0.44°
Hybrid/40	Hybrid/27	Hybrid/40	Hybrid/19	Terrain-following ETA/28	Hybrid/56
Semi-Lagrangian 720	Semi-Lagrangian 240	Semi-Lagrangian 1200	Eulerian 300	Eulerian 240	Semi-Lagrangian 1200
Tiedtke (1989)	Tiedtke (1989)	Kain and Fritsch (1990, 1993)	Gregory and Rowntree (1990); Gregory and Allen (1991)	Kain (2004)	Kain and Fritsch (1990); Kuo (1965)
Fouquart and Bonnel (1980)	Morcrette et al. (1986); Giorgetta and Wild (1995)	Savijärvi (1990); Sass et al. (1994)	Edwards and Slingo (1996)	Dudhia (1989); Mlawer et al. (1997)	Li and Barker (2005)
Eddy-diffusivity (first-order K) mass flux approach	Louis (1979)	Cuxart et al. (2000)	Wilson (1992)	Hong et al. (2006)	Benoit et al. (1989); Delage (1997)
Tiedtke (1993)	Lohmann and Roeckner (1996)	Rasch and Kristjánsson (1998)	Smith (1990)	WSM5; Hong et al. (2004)	Sundqvist et al. (1989)
TESSEL; ECMWF (2007)	Hagemann (2002); Rechid et al. (2009)	Samuelsson et al. (2006)	MOSES2; Essery et al. (2003)	Smirnova et al. (2000)	CLASS 3.5 Verseghy (2000)
van Meijgaard et al. (2008); based on ECMWF cycle 31r1; ECMWF (2007)	Jacob (2001); Jacob et al. (2007)	Samuelsson et al. (2011)	Jones et al. (2004)	Skamarock et al. (2008)	Zadra et al. (2008)

et al. 2004). Figure 2 shows GPCP precipitation for the January–March (JFM) season and deviations from GPCP in the other observational datasets and ERAINT. Figure 2 indicates that TRMM has a large dry bias over southern tropical Africa compared to GPCP, with relative differences of as much as 50% in some regions. The gauge-based precipitation datasets and GPCP show much better consistency, although some significant differences can still be seen on smaller spatial scales. Similar results hold for other seasons (not shown), with a common tendency for TRMM to have less precipitation than GPCP and the gauge products to be in better agreement. ERAINT precipitation is heavily biased (wet) compared to differences among the observations.

The large difference between TRMM and GPCP is explained by the fact that both products are adjusted to large-scale monthly precipitation from gauge networks but use different gauge analysis products. TRMM (version 6) is adjusted to the old GPCC gauge analysis ''monitoring product'' (version 2) for 1998–April 2005 and to the Climate Anomaly Monitoring System (CAMS) gauge analysis product (Xi et al. 1996) thereafter (Huffman and Bolvin 2011). GPCP (version 1.1) is scaled to the GPCC version 4 product using the full analysis up to 2007 and the monitoring product thereafter (Huffman et al. 2009). Globally, the shift from the old GPCC to the newer version 4 causes a 7% increase in precipitation over land in GPCP, with a pronounced increase over Africa (Huffman et al. 2009). The spread among the pure ground-based products (UDEL, CRU, GPCC), which partly share the same gauge stations, may arise from different processing algorithms and different levels of station availability in given time periods, especially in regions with very few or no stations (Yin and Gruber 2010). For example, a detail analysis of the number of gauge stations included in the GPCC product shows that almost no stations report observations over central Africa (primarily Angola, Democratic Republic

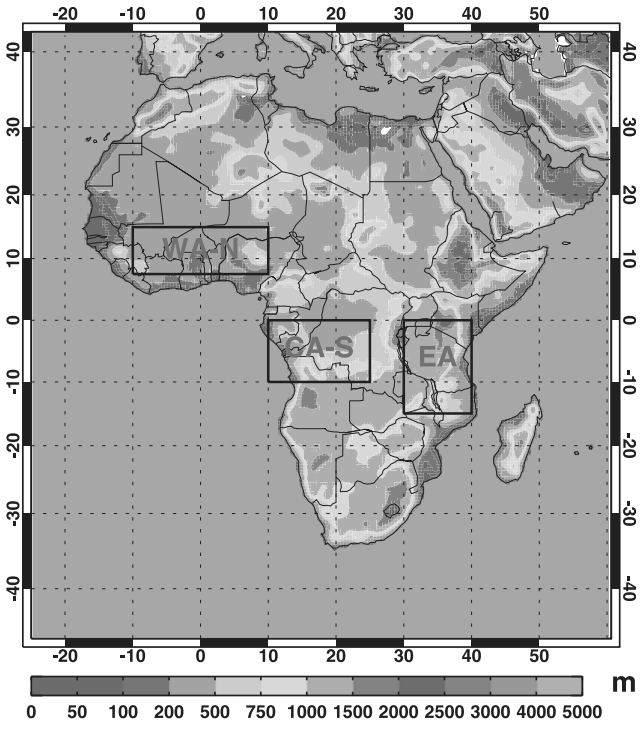

FIG. 1. The CORDEX-Africa domain at 50-km resolution, with topography (m) and three subregions used for spatially averaged analysis also plotted.

of the Congo, Tanzania, and Mozambique; see Fig. 3), the region with maximum rainfall in JFM, for all months in the 1998–2008 period. In these regions it is difficult to quantify uncertainties among the observational datasets in terms of which one is more realistic. Because of its use of a more recent gauge dataset for large-scale scaling, we decided to use GPCP as the reference dataset for the evaluation of the seasonal mean and annual cycle, despite its relatively coarse resolution. For evaluation of the diurnal cycle both TRMM and CMORPH are utilized, although the reader should keep in mind that the current version of TRMM may underestimate precipitation amounts. One possible approach for future analysis may be to simply apply an ensemble average to all observational datasets as a reference while retaining an estimate of the interobservational spread, at least for evaluation of the seasonal mean over land.

4. Seasonal mean precipitation

Figures 4 and 5 show GPCP precipitation for the July–September (JAS) and JFM seasons and differences from GPCP in the other observational datasets, the 10 RCM simulations, as well as ERAINT and the RCM multimodel ensemble. In JAS (Fig. 4) the rain belt associated with the intertropical convergence zone (ITCZ) reaches its most northerly location, stretching from the mountains of Darfur in East Africa to the Guinea Highlands and downstream into the Atlantic. Compared to GPCP, UDEL and GPCC are in good agreement with some tendency for smaller precipitation amounts, while TRMM has a large underestimate over East Africa and the Guinean Highlands and an overestimate over the Cameroon Highlands. As expected, the RCM biases are very diverse and vary significantly across the individual simulations. All RCMs capture the large-scale patterns of JAS precipitation (not shown) but have larger biases than the spread across the GPCP, UDEL, and GPCC products. Nevertheless, biases in many of the RCMs are of comparable magnitude to differences between the TRMM and GPCP observations. The largest differences in JAS are found in West Africa over the Guinean Highlands and downstream, with some models (HIRHAM, REMO, WRF, CRCM) strongly overestimating precipitation, one (ARPEGE) strongly underestimating, and one [the Consortium for Small-Scale Modeling (COSMO) model in climate mode (CCLM)] showing large, oppositely signed biases in a dipole pattern. Almost all RCMs have a large positive precipitation bias northeast of Madagascar. This is an area where significant observed precipitation interacts with the RCM lateral boundary and may, therefore, reflect problems in representing convection in the RCM boundary relaxation zones, where artificial dynamical imbalances can lead to low-level convergence and excessive convection. Ocean–atmosphere coupling may also improve the simulated precipitation over the Indian Ocean, as shown by Ratnam et al. (2009) in coupled and uncoupled experiments with RegCM3.

In the JFM season, the ITCZ reaches its most southerly location (Fig. 5), with maxima in southern tropical Africa and Madagascar. Most of the conclusions for JFM are similar to JAS: UDEL and GPCC are in better agreement with GPCP than TRMM, which has a dry bias over land. The RCMs biases vary significantly between individual simulations, with biases again generally larger than across the observation datasets. One common feature is a significant negative bias over Madagascar in most of the RCMs relative to GPCP, which is also seen in the majority of the alternative observation datasets. Many of the RCMs again show positive precipitation biases close to the eastern boundary, collocated with an observed precipitation maximum.

For both seasons the RCM ensemble average outperforms nearly all the individual models, with biases comparable to differences between the observational datasets. Figures 4 and 5 clearly show that much of this good performance of the ensemble mean results from the cancellation of oppositely signed biases, a number of which may reflect precipitation placement errors. The

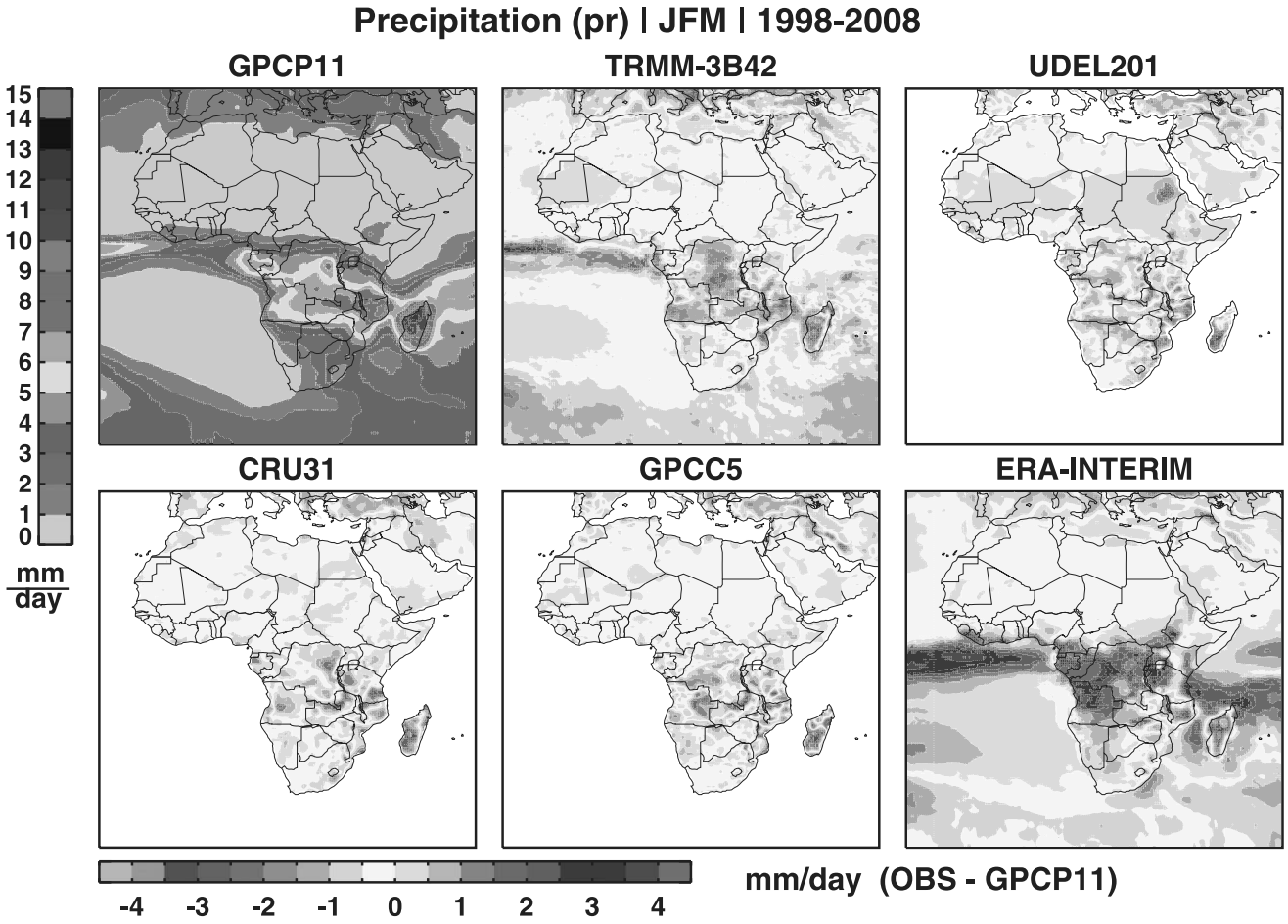

FIG. 2. GPCP mean JFM precipitation (1998–2008) and differences between other gridded precipitation products and GPCP.

ensemble mean substantially improves the ERAINT precipitation (see also Paeth et al. 2011). Moreover, many individual RCMs have more accurate precipitation than the ERAINT data, which were used as lateral and surface boundary conditions.

To evaluate the seasonal progression of the ITCZ, we use a simple method to approximate its position by calculating the geographical position of maximum precipitation in the center of the rain belt and the 1 mm day^{-1} mean intensities on either flank of this maximum. Figure 6 plots the ensemble mean, seasonal mean, and precipitation bias with respect to GPCP for all four seasons, together with the approximated position of the ITCZ. While individual RCMs have localized placement errors in terms of the ITCZ seasonal progression, through the cancellation of these errors, the RCM ensemble mean has an extremely accurate estimate of the location of the ITCZ and the maximum precipitation within the ITCZ in all four seasons.

As well as representing seasonal mean climatological precipitation, it is important that RCMs capture the observed interannual variability in precipitation, particularly the variability associated with large-scale modes of the coupled climate system, such as El Niño–Southern Oscillation (ENSO) forced modes. Figure 7 displays time series of the spatially averaged, seasonal mean normalized precipitation for three regions: northern West Africa (7.5°–15°N, 10°E–10°W), southern central Africa (10°–0°S, 10°–25°E), and East Africa (15°–0°S, 30°–40°E) as illustrated in Fig. 1. Over West Africa interannual precipitation variability is in very good agreement across the observational datasets. All of them show the same extremely wet or dry years relative to the 1990–2008 climatology, with a small difference in magnitude in some years. ERAINT does not reproduce the observed interannual variability over this region and has an artificial trend not seen in observations. The RCM ensemble average substantially improves on ERAINT, more closely following the observed variations, albeit failing to reproduce 1994, 1995, and 2008. Spread across the observations is larger in East Africa, where one of the observational dataset can show an extremely wet/dry year while others show the same year close to the climatology, for example, 1994, 2002, 2005, and 2007. Both

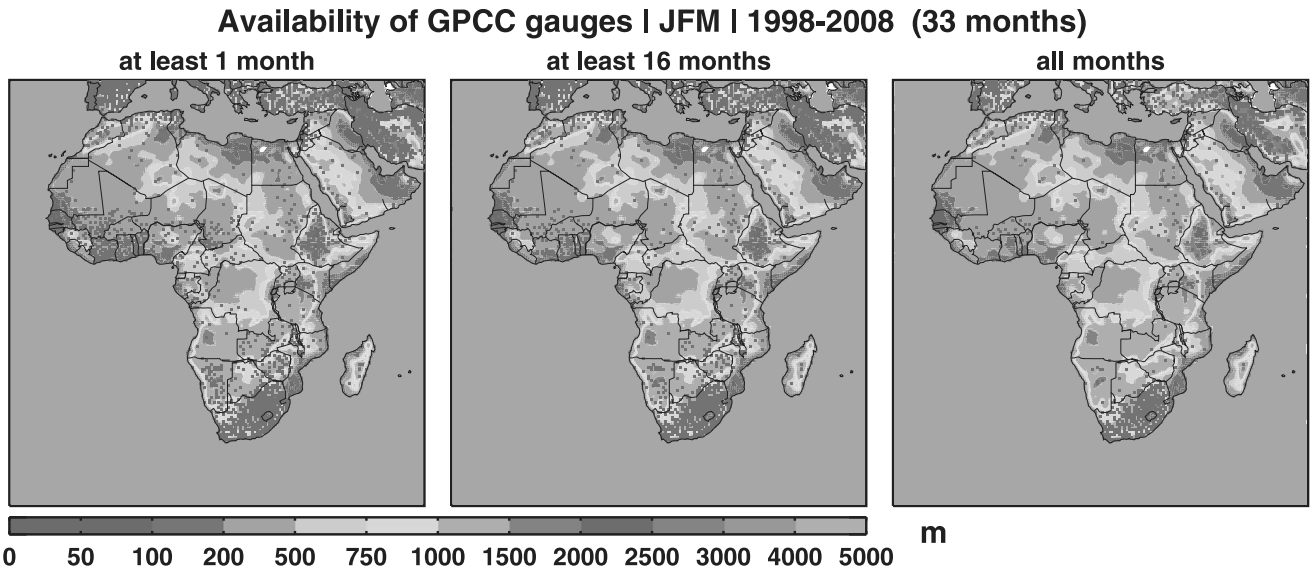

FIG. 3. Availability of the GPCC gauge stations in JFM (1998–2008). Red dots show that at least one gauge per grid box is available (left) for at least one month, (middle) for at least 16 months (about half of the period), and (right) for all 33 months. Color shows 50-km resolution topography (m).

the ERAINT and the ensemble mean, in general, follow the observational envelope but both or one of them fail to reproduce some wet/dry years when the observations are in agreement (1992, 2000). Observational uncertainties are even larger in central Africa compared to East Africa, and for many individual years it is impossible to conclude whether it is a wet or dry year. In addition, the CRU precipitation shows no interannual variability at all in 2002–08 in contrast to the GPCC and UDEL. Such large uncertainties among the CRU, UDEL, and GPCC datasets, most likely related to there being almost no observational stations in central Africa (see Fig. 3), preclude us from evaluating the interannual precipitation variability over this region.

5. West African monsoon rainfall

It is a challenging task for both global and regional climate models to simulate the range of complex processes that make up the WAM (Cook and Vizy 2006; Druyan et al. 2010; Xue et al. 2010; Ruti et al. 2011). In Fig. 8 we plot the observed and simulated annual cycle of precipitation averaged between 10°E and 10°W. Such a figure depicts the latitudinal progression of the main WAM rainfall, as well as its seasonal intensification and decay. GPCP and TRMM represent the well-known behavior of the WAM: maximum rainfall at the end of May/beginning of June over the Gulf of Guinea (0°–6°N) followed by an abrupt northward jump from the Gulf of Guinea to the Sahel, with the establishment of a new maximum around 10°N in August and a southward retreat thereafter (Sultan and Janicot 2000; Janicot 2009). While the temporal and spatial details are generally similar in both datasets, TRMM exhibits higher rainfall intensities over the Gulf of Guinea, south of 5°N, and slightly lower intensities over the Sahel. ERAINT reproduces the large-scale features of the WAM rainfall but differs in rainfall intensities and, in particular, fails to propagate precipitation far enough north in July–August, resulting in a significant dry bias between ~10° and 18°N. The individual RCMs reproduce the WAM rainfall with varying degrees of accuracy. Most RCMs capture the two rainfall maxima, over the Gulf of Guinea and the Sahel, although the positioning, intensity, and duration of these maxima differ across the models. Seven of the models [Rossby Centre regional atmospheric model (RCA), HIRHAM, CCLM, REMO, Royal Netherlands Meteorological Office (KNMI) Regional Atmospheric Climate Model (RACMO), Providing Regional Climates for Impacts Studies (PRECIS), and WRF] simulate a northward jump in precipitation from the Gulf of Guinea to the Sahel region, at roughly the correct time of the year, although with varying degrees of accuracy. Four models (HIRHAM, REMO, CCLM, and PRECIS) show a second maximum over the Gulf of Guinea in November that resembles a ''southward jump'' of the WAM, while a more gradual retreat is evident in the observations. Three of these RCMs (HIRHAM, REMO, and CCLM) strongly overestimate rainfall maxima both in May–June and October–November. Some models show very weak maxima: CCLM in Sahel, RegCM3 over the Gulf of Guinea, or no maximum at all as in ARPEGE in the

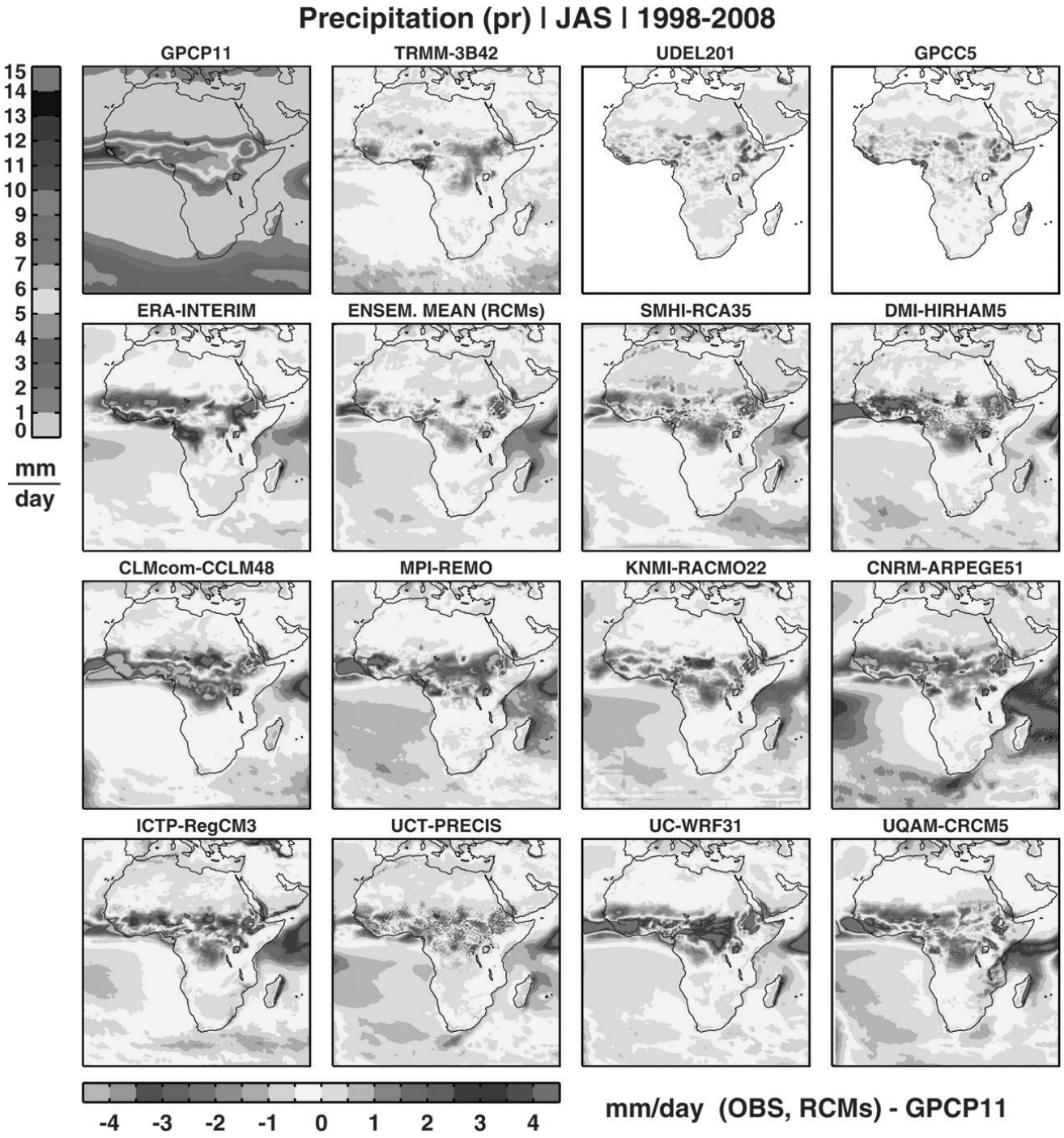

FIG. 4. GPCP mean JAS precipitation for 1998–2008 and differences compared to GPGP in the other gridded observations, the individual RCMs, and their ensemble average.

Sahel. Three models (RCA, ARPEGE, and CRCM) do not propagate WAM precipitation sufficiently far north. The multimodel average smoothes these diverse biases and presents the best simulated WAM precipitation. Despite some overestimation of rainfall in May–June, the shape and intensity of the annual cycle is quite accurate, with some evidence of a slight underestimate of the northward extension and the existence of an erroneous secondary jump/maximum in October–November. The RCM ensemble mean WAM rainfall is a significant improvement over that associated with the ERAINT driving data.

6. Annual cycle

Figure 9 displays the spatially averaged, mean annual cycle of precipitation over the West, central, and East

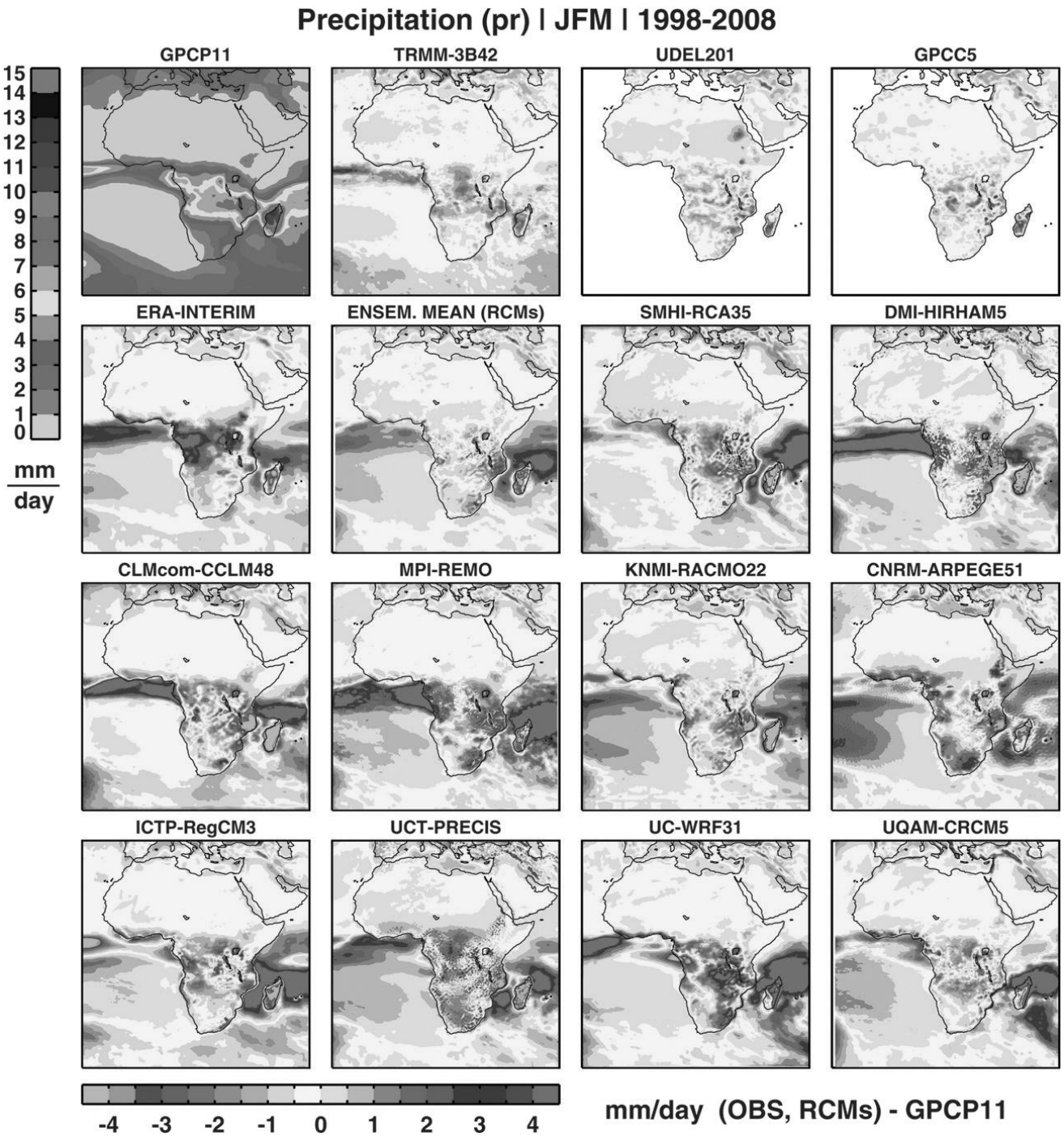

FIG. 5. As in Fig. 4, but for JFM.

Africa regions illustrated in Fig. 1. The annual cycle over West Africa (left column) depicts the prominent features of precipitation in this region associated with the seasonal migration of the WAM: dry in the boreal winter and a rainy season from May to October, with maximum precipitation in late August. GPCP and TRMM are close to each other, although GPCP has systematically somewhat higher precipitation rates than TRMM. Individual RCM simulations in the spaghetti plot (top, left) show a wide spread around the observed annual cycle with some significant overestimates (HIRHAM, WRF, and RegCM3) and underestimates (ARPEGE and CCLM) during the development and maximum phase of the WAM. Much better agreement is seen between the RCMs and observations during the decay of the rainy season (October–November). A common tendency during the

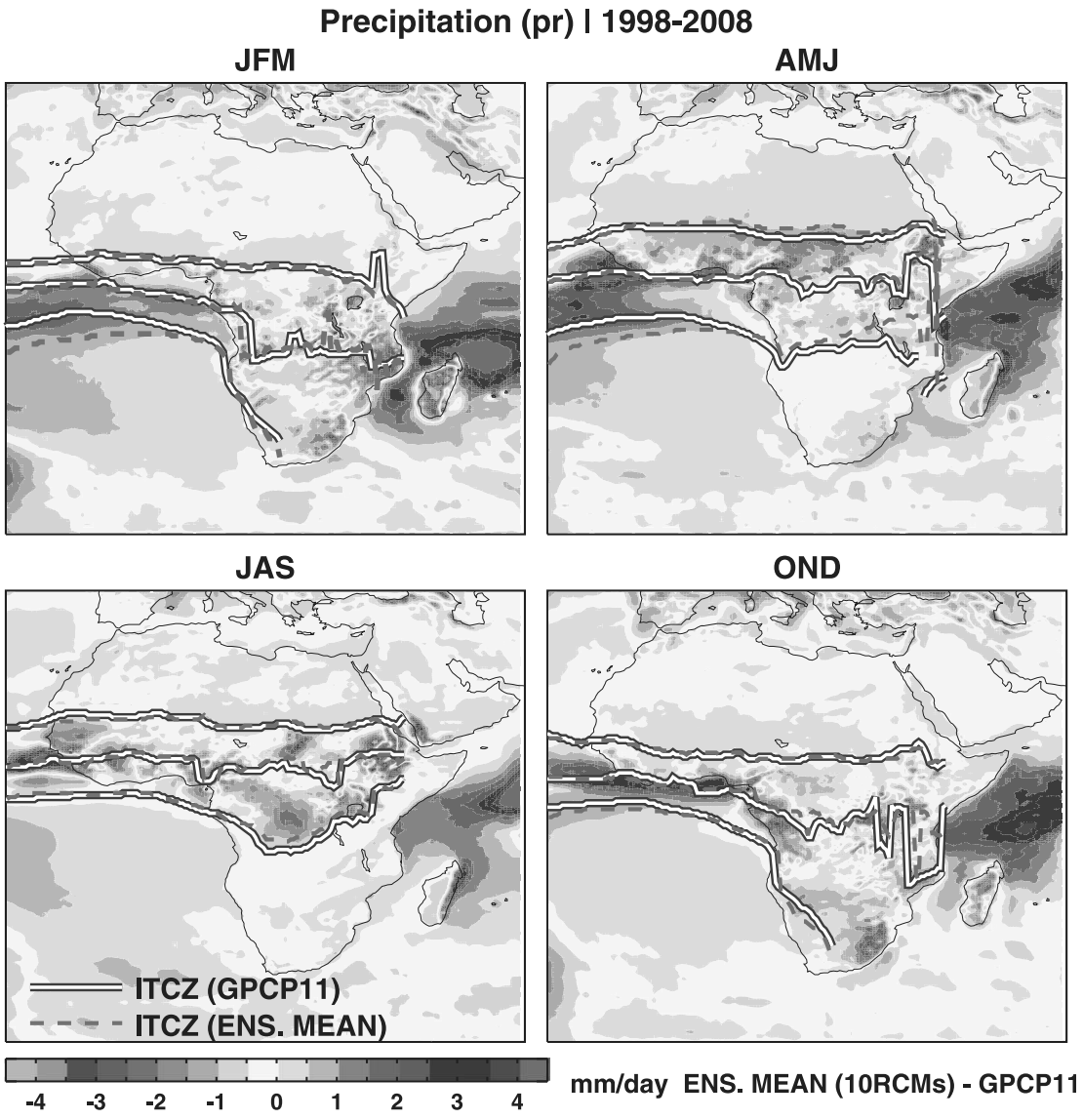

FIG. 6. The ensemble mean precipitation bias relative to GPCP for four seasons [including April–June (AMJ) and October–December (OND); color] and the approximate position of the ITCZ in GPCP precipitation (blue–white line) and in the RCM ensemble mean (red dashed line).The ITCZ position is defined as the maximum precipitation in the center of the rain belt and 1 mm day^{-1} on its flanks.

onset is that most RCMs overestimate precipitation, indicating a too-early start of the rainy season by about one month (e.g., RCA, ARPEGE, and PRECIS). The ensemble mean reproduces the common tendency of the RCMs to overestimate precipitation during the onset but otherwise accurately represents the observed annual cycle, although again we emphasize error cancellation across individual RCMs leads to the accurate ensemble mean estimate. Again, several RCMs and particularly the ensemble mean improve on ERAINT, which has large dry bias during the rainy season. In the bottom row of Fig. 9, we reproduce the same spatial mean, annual cycle plots, but now the full range of the RCM results is plotted in gray shading, while the 25th–75th percentile range is shown in yellow. For West Africa (bottom, right) removing the outlier models significantly improves the accuracy of the ensemble precipitation.

In central Africa the distinctive feature is the bimodal structure of the annual cycle, with maxima in November and March–April (middle column). Similar to West Africa, both GPCP and TRMM have the same shape of the annual cycle with slightly higher intensities in GPCP. All RCMs capture the basic shape of the annual cycle, on average underestimating the first maximum and overestimating the second. Nearly all the RCMs simulate precipitation more accurately than ERAINT, which

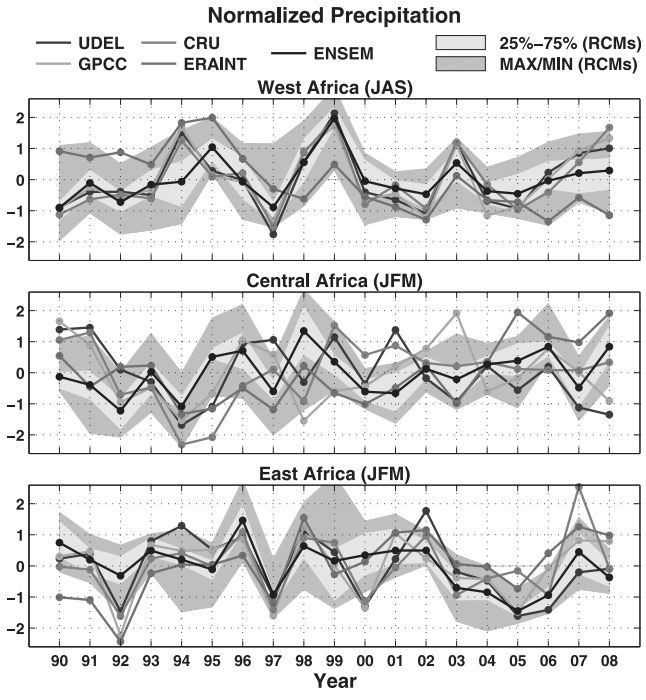

FIG. 7. Seasonal mean normalized precipitation over (top) northern West Africa (7.5°–15°N, 10°W–10°E), (middle) southern central Africa (10°–0°S, 10°–25°E), and (bottom) East Africa (15°–0°S, 30°–40°E). Gray shading is the full range of the RCM results, and yellow shading is the 25th–75th percentile range.

has too-intense rainfall throughout the year. The ensemble mean and the 50% most accurate RCMs closely follow the observed annual cycle.

Over East Africa (right column), where maximum rainfall occurs in the boreal winter, ERAINT overestimates precipitation, while individual RCMs again show various behaviors grouped around the observations, with the ensemble average again leading to an accurate representation of the annual cycle.

7. Diurnal cycle

The diurnal cycle is a prominent forced mode of atmospheric variability that can significantly modulate regional, near-surface thermal, and hydrological regimes. Many studies have shown that global and regional climate models generally have a poor representation of the diurnal cycle of precipitation, suffering from biases in the frequency of precipitation occurrence, precipitation intensity, and the timing of rainfall during the day (e.g., Dai et al. 1999; Dai and Trenberth 2004; Shin et al. 2007; da Rocha et al. 2009; Jeong et al. 2011). In the tropics, the main features of the diurnal cycle have been well documented from ground- and satellite-based observations and include a late afternoon/evening maximum over land and an early morning maximum over open ocean (Dai 2001; Yang and Slingo 2001; Yang and Smith 2006; Dai et al. 2007). Figure 10 plots the local time of maximum rainfall in the diurnal cycle for the JAS season, with the black lines indicating the extent of the ITCZ for this season, as depicted in Fig. 5. While there is a fair amount of small-scale variability, both TRMM and CMORPH indicate rainfall maxima between late afternoon and midnight, or even later. The near-midnight maximum is related to the fact that the majority of precipitation produced in the ITCZ region during this season is produced by mesoscale convective systems. These are usually initiated around 1700–1800 local solar time (LST) but precipitate at maximum intensity later in the day, during their mature phase (McGarry and Reed 1978; Hodges and Thorncroft 1997). ERAINT precipitates too early, with the widespread occurrence of maximum precipitation intensity around local noon. The majority of RCMs exhibit the same out-of-phase diurnal cycle, with only RCA and CRCM capturing to some degree the observed phase of the diurnal cycle.

The diurnal cycle of precipitation is sensitive to the convective parameterization used (Dai et al. 1999; Liang et al. 2004). One possible explanation for the more realistic diurnal cycle in RCA and CRCM is that both models employ the Kain–Fritsch (KF) convection scheme (Kain and Fritsch 1990; Bechtold et al. 2001), while ERAINT and most of the other RCMs have different schemes (see Table 1). Liang et al. (2004) evaluated the diurnal cycle of precipitation over the United States in a regional model and found the KF scheme to be more accurate than the Grell scheme (Grell 1993) in representing late afternoon rainfall peaks when moist convection is controlled by near-surface forcing. However, it is not clear why WRF, which also has the KF scheme, precipitates too early.

A more detailed analysis of the diurnal cycle, spatially averaged over West, central, and East Africa is presented in Fig. 11. In West Africa for the JAS season, TRMM and CMORPH show basically the same shape and amplitude of the diurnal cycle, with an evening to midnight maximum. CMORPH generally has higher precipitation intensities than TRMM. Only one model—CRCM—captures both the shape and amplitude of the observed diurnal cycle, while RCA has a too-flat diurnal cycle over this region. In agreement with Fig. 10, convective precipitation in all other models and ERAINT is triggered too early, between 0800 and 1000 LST with maximum precipitation rates generally occurring around local noon. REMO has the latest maximum of this group, with peak intensities at 1500 LST. The ensemble mean can partly correct the amplitude of the diurnal cycle, which is very different among the individual simulations but not the phase, with a maximum between 1300 and 1400 LST. Similar behavior is evident over both central and East Africa for

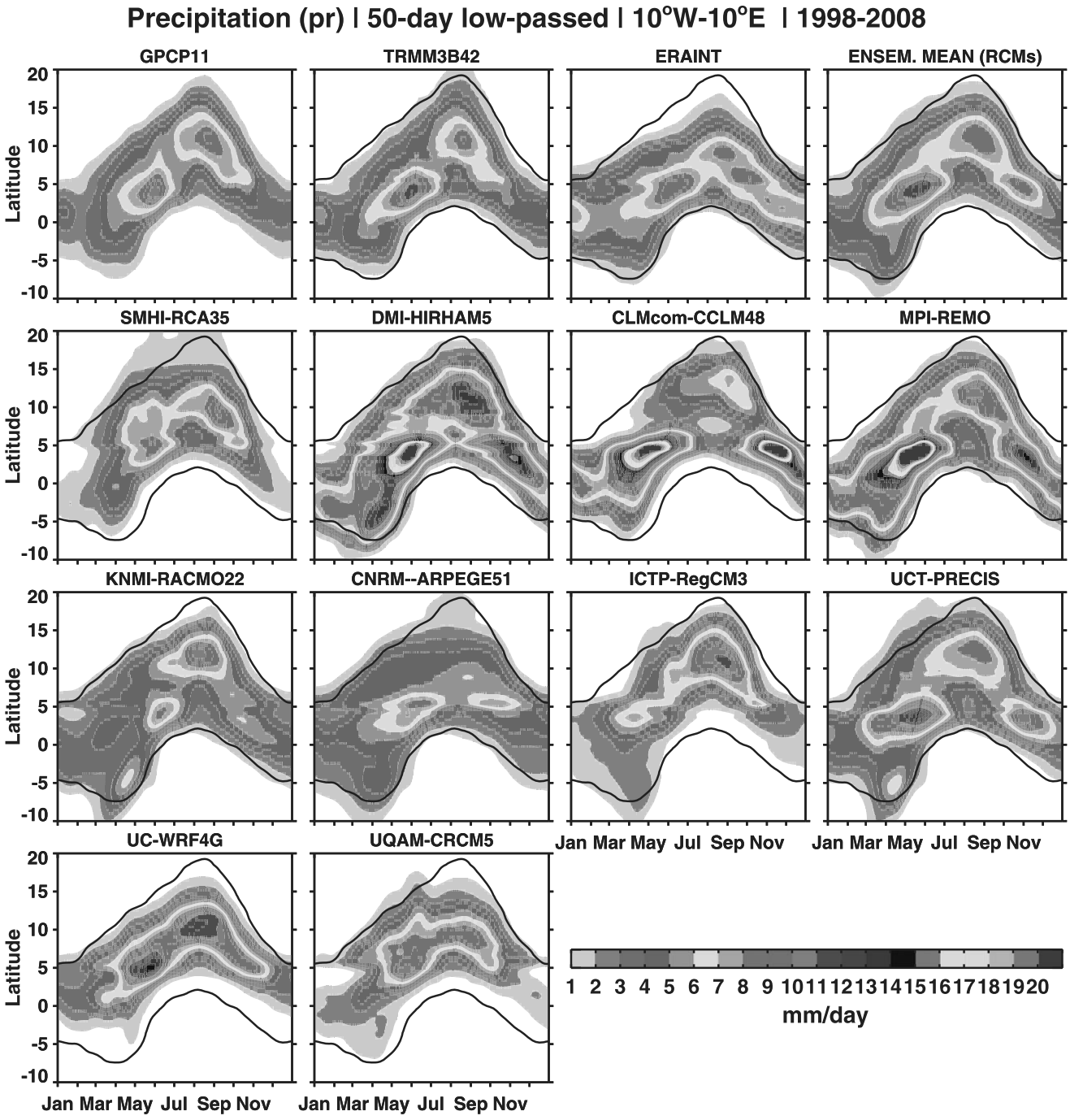

FIG. 8. Seasonal march of the 50-day low-passed precipitation averaged over 10°E–10°W. Black lines, as a reference, are 1 mm day^{-1} contours from GPCP.

the DJF season (Fig. 11), where the observed rainfall maximum occurs between 1700 and 1800 LST. Again, CRCM has the most accurate diurnal cycle, with RCA having a more pronounced diurnal cycle over these two regions, although with peak intensities 2–3 h too early. ERAINT and all other RCMs again have maximum rain rates around local noon, which is also seen in the ensemble average.

One approach, to better understand the diurnal cycle of precipitation, is the use of frequency–intensity plots (FI) based on 3-hourly data. Figure 12 shows 3-hourly FIs for TRMM, CMORPH, ERAINT, and all models over the West Africa region. The figure depicts the mean diurnal cycle of the frequency of occurrence of different precipitation intensities. In both TRMM and CMORPH, there is a clear peak in the occurrence of light/zero rain

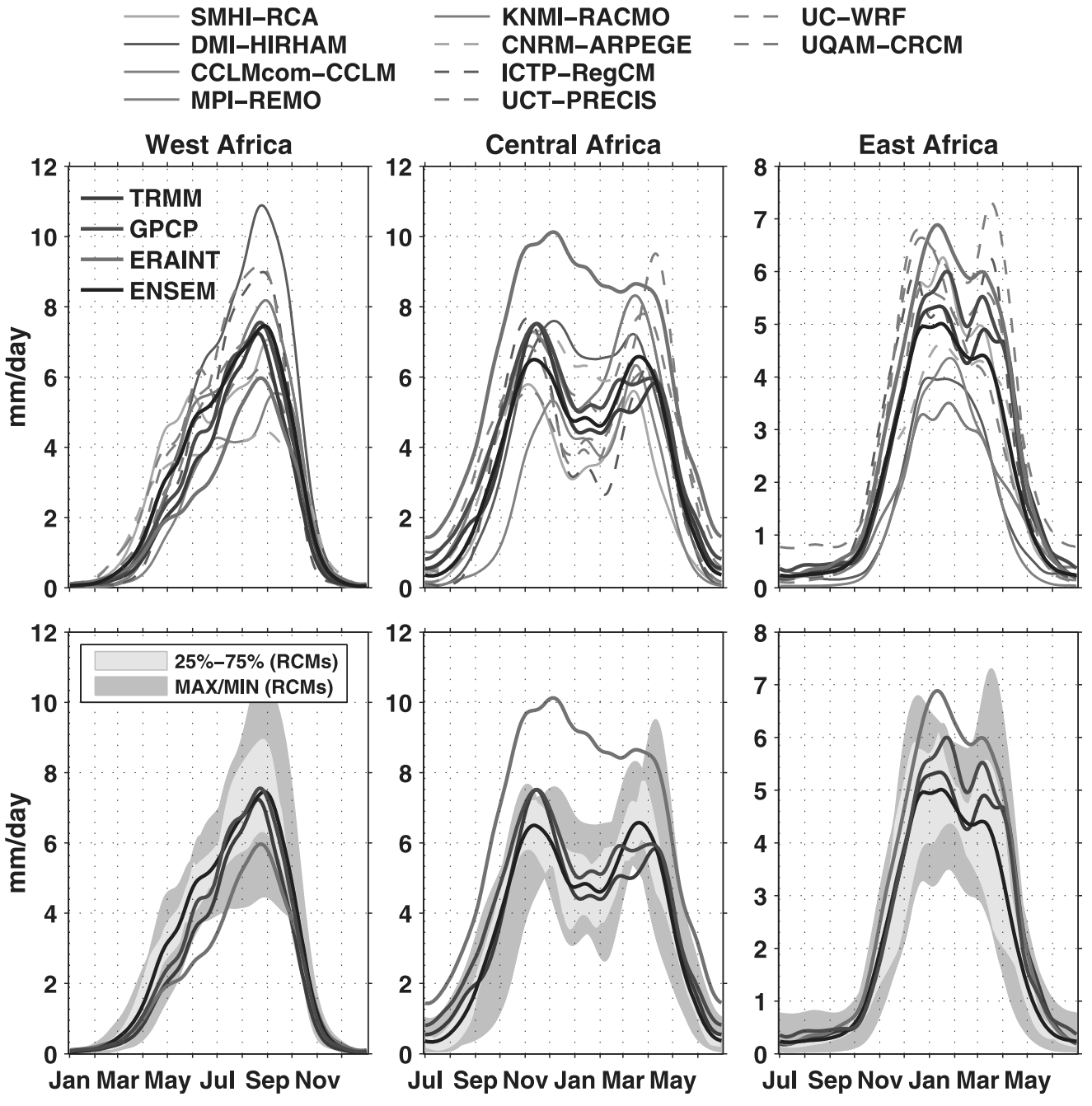

FIG. 9. Annual cycle of the 50-day low-passed precipitation (1998–2008) averaged over (left) northern West Africa (7.5°–15°N, 10°W–10°E), (middle) southern central Africa (10°–0°S, 10°–25°E), and (right) East Africa (15°–0°S, 30°–40°E). Gray shading is full range of the RCM results, and yellow shading is the 25th–75th percentile range.

rates from ~0800 to 1500 LST (the red area on the figure) and a temporally collocated minimum in the occurrence of heavier rain rates in excess of 1 mm 3 h^{-1}. Between ~1800 and 2100 LST, both observations now indicate a minimum in the occurrence of light/zero rain rates and a relative maximum in intensities greater than ~0.5 mm 3 h^{-1}.

ERAINT is almost a mirror image of TRMM, with completely the opposite phase; the highest frequency of light/zero rainfall between 1800 and 0800 LST; and the maximum occurrence of intense precipitation around local noon. Four RCMs—HIRHAM, RACMO, CCLM, and REMO, which all employ different versions of the Tiedke convection scheme—show similar diurnal intensity distributions to ERAINT, which also has the Tiedke scheme employed in the ECMWF model used to generate ERAINT. Of the three models employing the KF scheme (CRCM, RCA, and WRF), only CRCM captures the

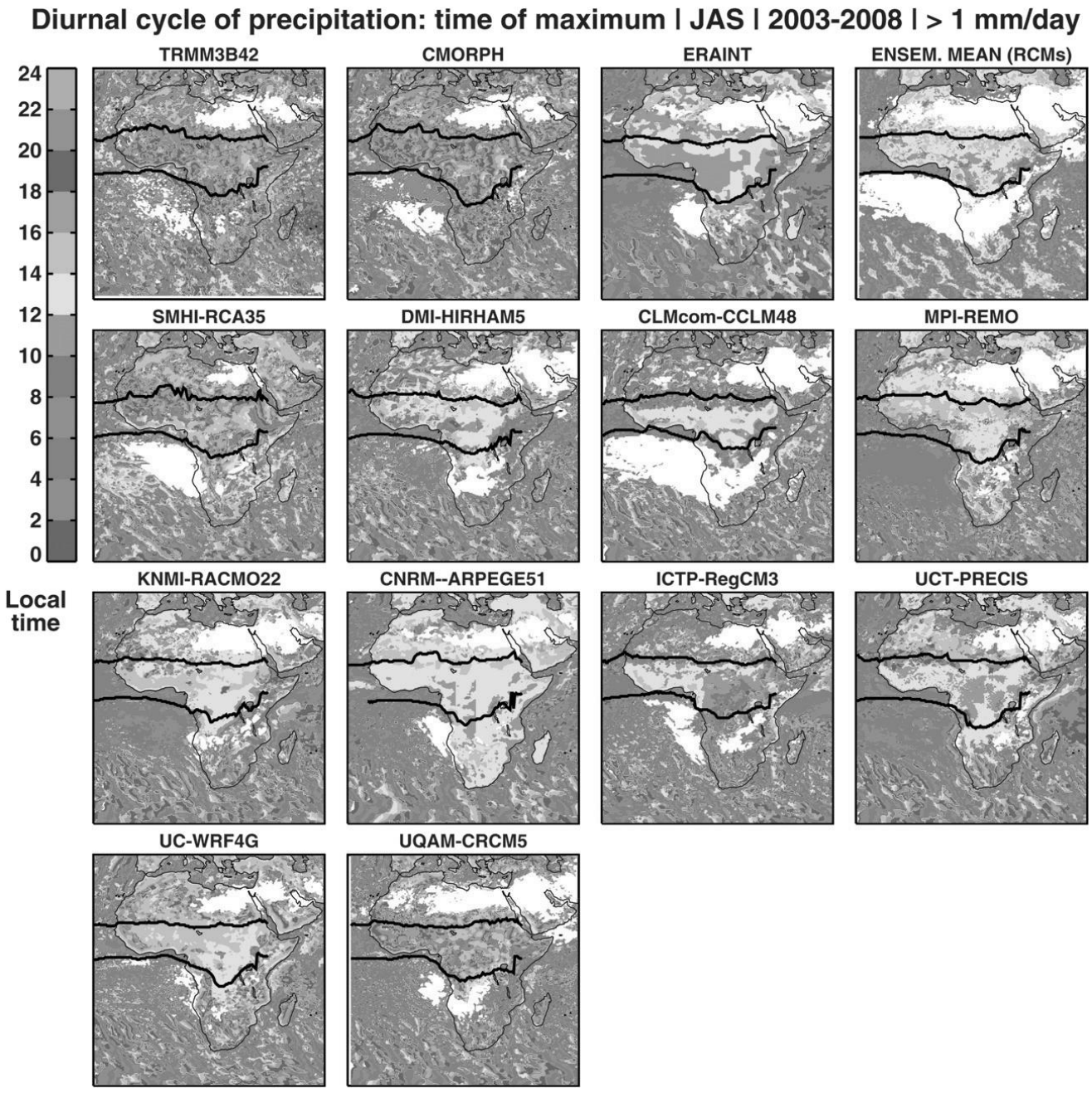

FIG. 10. LST of maximum precipitation intensity during the diurnal cycle for JAS (2003–08). Time of maximum precipitation is based on a cubic spline fitted to the 3-hourly precipitation. Black lines are the 1 mm day^{-1} contour (JAS mean) for each respective dataset, showing the approximate position of the ITCZ. White colors denote areas where there are no days with rainfall more than 1 mm day^{-1} in the JAS season.

main features of the observed FIs, while RCA has a too-flat distribution and WRF, somewhat puzzlingly, has a distribution very similar to models employing the Tiedke scheme. All other RCMs with different convective schemes (ARPEGE, RegCM3, and PRECIS) have FIs similar to the Tiedke family of models, with the highest frequency of light/zero rainfall between late afternoon and morning and the maximum occurrence of intense precipitation centered at local noon. Figure 12 emphasizes the main RCM deficiency in simulating precipitation over Africa remains a poor representation of the diurnal cycle. Models employing the KF scheme appear to do better in this regard; two possible factors contributing to this improvement may include (i) the use of an advanced convective trigger function and (ii) that entrainment and detrainment processes are responsive to environmental conditions, through the buoyancy sorting approach (Kain and Fritsch 1990). More research is

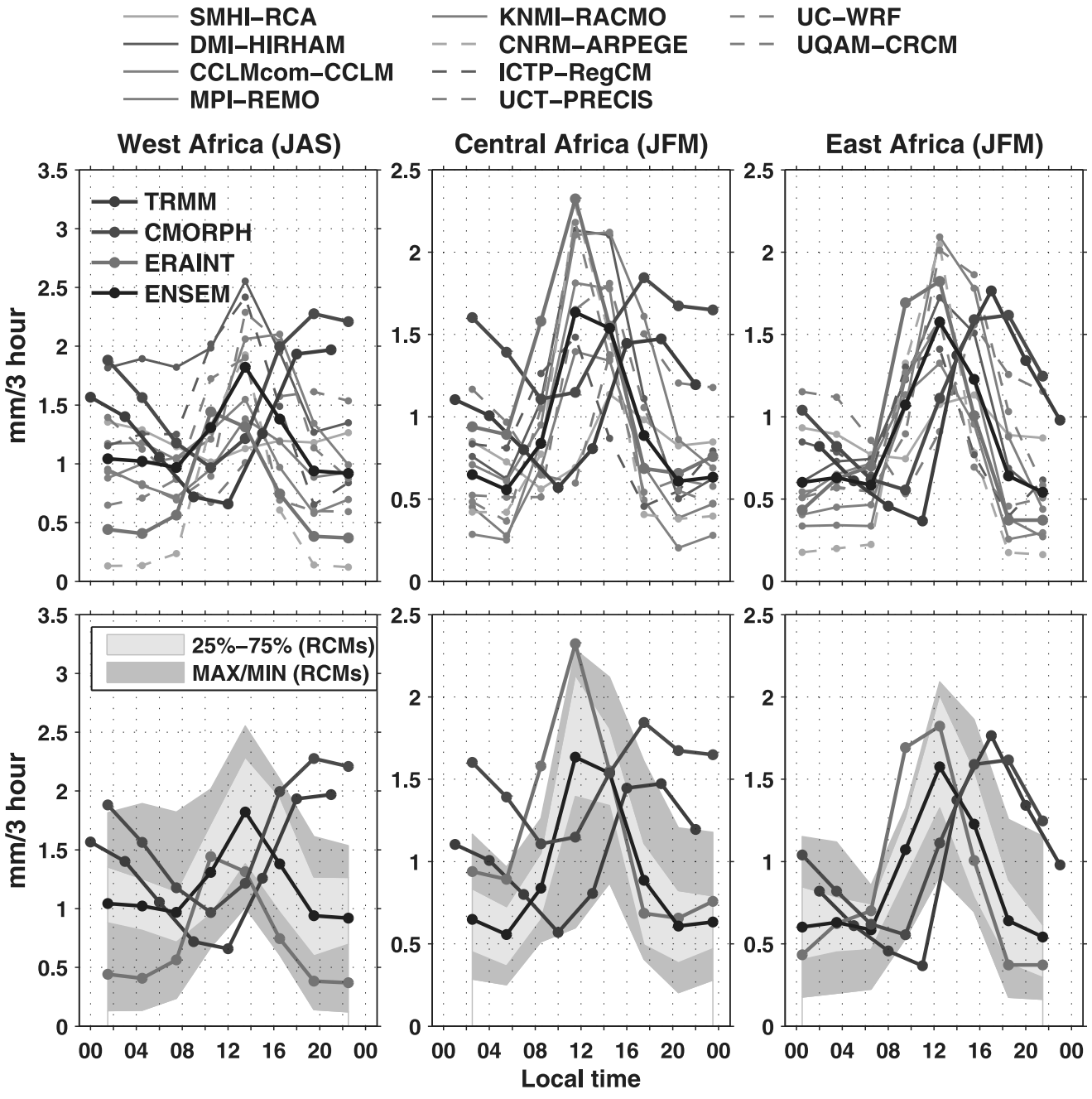

FIG. 11. Diurnal cycle of precipitation over (left) northern West Africa (7.5°–15°N, 10°W–10°E), (middle) southern Central Africa (10°–0°S, 10°–25°E), and (right) East Africa (15°–0°S, 30°–40°E) for the 2003–08 period. Gray shading is the full range of the RCM results, and yellow shading is the 25th–75th percentile range.

planned to understand the factors behind the good representation of the diurnal cycle in the CRCM model and differences seen relative to RCA. These findings may help improve the diurnal cycle in some of the other RCMs.

8. Summary and conclusions

We present a first evaluation of the precipitation climatology over the African continent in an ensemble of regional climate simulations performed within the CORDEX-Africa project. The ensemble consists of 10 different RCMs all run at ~50-km resolution, on a common grid, and driven by ERA-Interim for the period 1989–2008. Performance of the individual models and the ensemble average is evaluated in detail for different aspects of African precipitation, namely, seasonal means, West African monsoon rainfall, and annual and diurnal cycles.

Several gridded precipitation products, based on ground and/or satellite-derived observations, are included in the

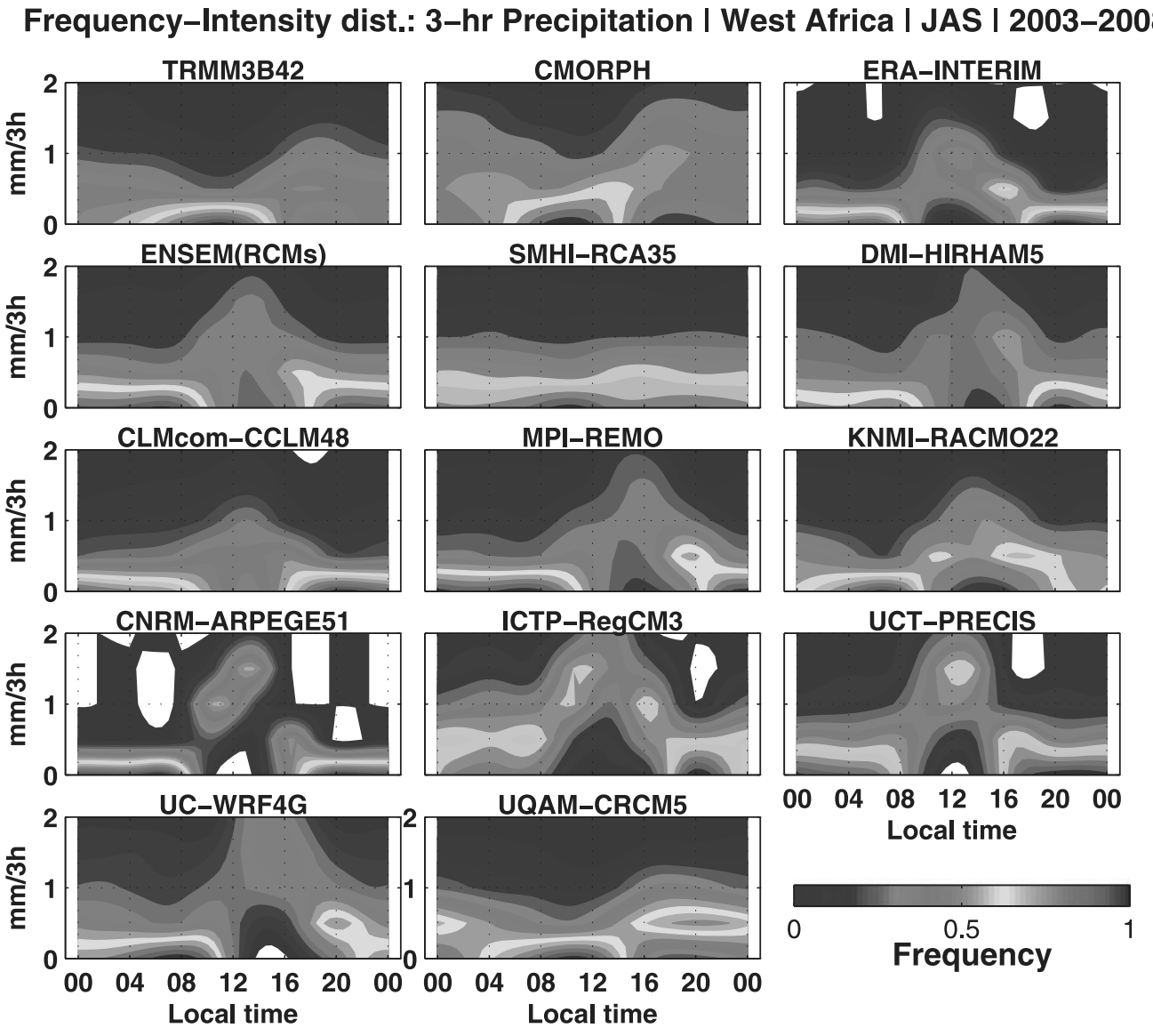

FIG. 12. Diurnal cycle of FI distribution of precipitation based on the 3-hourly data averaged over northern West Africa (7.5°–15°N, 10°E–10°W) in JAS (2003–08).

evaluation to encompass uncertainties in the observational data. Intercomparison at seasonal mean time scales reveals that two satellite products—TRMM and GPCP—can differ by as much as 50% over large areas due to the adjustment of large-scale satellite estimates to different gauge products. Differences between pure gauge products—CRU, UDEL, GPCC—and the combined satellite–gauge dataset GPCP are, on average, smaller than differences between TRMM and GPCP. It is not possible to derive a thorough estimate of the quality of the gauge products as they are not independent of each other. Furthermore, there are very few or no reporting gauge stations over large parts of Africa. Interannual precipitation variability over regions of low surface observational density is very different across the gauge products, although climatological estimates for sufficiently long periods are more consistent. An ensemble mean approach, similar to that employed with climate models, may partly improve the situation, by reducing random errors in the observational products.

On average all RCMs capture the main features of the seasonal mean rainfall distribution and its annual cycle, although significant biases can be found in individual models depending on region and season. The fact that individual model biases vary considerably in space and time has also been found in earlier multimodel studies for West Africa (Druyan et al. 2010; Paeth et al. 2011). The multimodel average generally, but not always, outperforms many of the individual models with biases of similar magnitude to differences between the observational datasets. Such good performance is mostly a result

of the cancelation of opposite-signed biases across the models. These findings are similar to those of Paeth et al. (2011) and emphasize the importance of using multimodel ensembles for simulating African climate. Nevertheless, many of the individual RCMs do improve the precipitation climate compared to their boundary condition dataset, ERA-Interim, which has biases significantly larger than the spread among the observations. Similar improvements over West Africa were also found by Paeth et al. (2011). Druyan et al. (2010) showed that for 4-yr simulations, initialized every year, all participating RCMs exhibited a positive precipitation bias, consistent with the bias in the boundary condition data—National Centers for Environmental Prediction–Department of Energy(NCEP–DOE) Reanalysis 2. This may be related to the short simulation period. The consistent improvement seen for the RCMs in this study indicates the potential advantage of applying high-resolution regional models which, by resolving small-scale processes, can improve on the large-scale boundary condition data in terms of societally important variables, such as precipitation.

Individual RCMs simulate WAM precipitation with differing levels of accuracy. Most capture the WAM rainfall maxima, over the Gulf of Guinea in late May–early June and in the Sahel region in August, although the positioning, intensity, and duration of these maxima differ across models. A number of the RCMs show a too-early onset of the WAM, but the majority captures its rapid northward progression into the Sahel by early July. Several models exhibit a second rainfall maximum over the Gulf of Guinea in November that is not supported by observations. As for the annual cycle, the multimodel ensemble mean generally outperforms individual RCMs, providing a significant improvement over the ERA-Interim WAM precipitation, which fails to propagate sufficiently far enough north.

The most challenging task over Africa remains the diurnal cycle of precipitation, with the majority of RCMs and ERA-Interim simulating a diurnal cycle completely out of phase with observations. The main problem appears to be related to the formulation of the convective parameterizations employed in the models, with a subset of the models that employ the Kain–Fritsch scheme showing a somewhat improved representation of the phase of the diurnal cycle. A thorough understanding of why these models show an improved diurnal cycle is deferred to a later study. When the ensemble mean is considered, the amplitude of the diurnal cycle is significantly improved but not the systematic bias in the phase. As projected climate changes may be sensitive to the diurnal precipitation characteristics (e.g., Lynn et al. 2007), model improvements, such as an improved diurnal cycle, may lead to more reliable future projections.

To summarize, most of the RCMs capture the main details of the precipitation climatology over Africa, although individual models do exhibit substantial biases depending on region, season, and evaluation metric. Overall, results of the first CORDEX evaluation over Africa are encouraging. For many of the RCM groups, this is the first experience of dynamical downscaling over Africa, where land–convection interactions play a leading role in defining details of the precipitation climate. The group of RCMs employed in this study will soon perform transient climate change projections within CORDEX, forced by coupled GCM results from CMIP5. This study provides the underlying assessment of the ability of these RCMs to describe African precipitation processes that are key to the management of freshwater resources and food security in the region.

Finally, we would emphasize that the ensemble average should not be viewed as the expected outcome in CORDEX-generated climate projections, although it outperforms most of the individual RCMs. Rather, we emphasize the need for a large ensemble of projections (as many as possible) to develop estimates of likelihood of occurrence based on agreement across the range of plausible AOGCM–RCM-simulated climate changes.

Acknowledgments. The authors thank the European Centre for Medium-Range Weather Forecasts (ECMWF), the Goddard Space Flight Center (GSFC), Climate Prediction Center (CPC), the British Atmospheric Data Centre (BADC), the University of Delaware, and the Global Precipitation Climatology Centre (GPCC) for providing observational data. Katja Winger (UQAM) and Neil MacKellar (DMI) are greatly acknowledged for preparing the model data. We would also like to thank George Huffman (GSFC) for providing detail information about the TRMM and GPCP datasets. Matthias Büchner is a representative of the CLM-Community CORDEX Africa group, consisting of Hans-Jürgen Panitz (KIT), Matthias Büchner (PIK), Alessandro Dosio (EC-JRC), Burkhardt Rockel (Helmholtz-Zentrum Geesthacht), Bodo Ahrens (University Frankfurt), and Andreas Will (BTU Cottbus). J. F. acknowledges financial support from the Spanish Ministry of Science and Innovation (CORWES Project CGL2010-22158-C02). We also thank three anonymous reviewers for their helpful comments.

REFERENCES

Afiesimama, E. A., J. S. Pal, B. J. Abiodun, W. J. Gutowski, and A. Adedoyin, 2006: Simulation of West African monsoon using RegCM3. Part I: Model validation and interannual variability. *Theor. Appl. Climatol.,* **86,** 23–27.

Alexandru, A., R. de Elia, R. Laprise, L. Separovic, and S. Biner, 2009: Sensitivity study of regional climate model simulations to large-scale nudging parameters. *Mon. Wea. Rev.,* **137,** 1666–1686.

Anyah, R. O., and F. H. M. Semazzi, 2007: Variability of East African rainfall based on multiyear RegCM3 simulations. *Int. J. Climatol.,* **27,** 357–371.

Baldauf, M., 2008: Stability analysis for linear discretisations of the advection equation with Runge–Kutta time integration. *J. Comput. Phys.,* **227,** 6638–6659.

——, and J.-P. Schulz, 2004: Prognostic precipitation in the Lokal Modell (LM) of DWD. *COSMO Newsletter,* No. 4, DWD, Offenbach, Germany, 177–180.

——, A. Seifert, J. Förstner, D. Majewski, M. Raschendorfer, and T. Reinhardt, 2011: Operational convective-scale numerical weather prediction with the COSMO model: Description and sensitivities. *Mon. Wea. Rev.,* **139,** 3887–3905.

Bechtold, P., E. Bazile, F. Guichard, P. Mascart, and E. Richard, 2001: A mass-flux convection scheme for regional and global models. *Quart. J. Roy. Meteor. Soc.,* **127,** 869–886.

Benoit, R., J. Côté, and J. Mailhot, 1989: Inclusion of a TKE boundary layer parameterization in the Canadian regional finit-element model. *Mon. Wea. Rev.,* **117,** 1726–1750.

Bougeault, P., 1985: A simple parameterization of the large-scale effects of cumulus convection. *Mon. Wea. Rev.,* **113,** 2108–2121.

Buzzi, M., M. W. Rotach, M. Raschendorfer, and A. A. M. Holtslag, 2011: Evaluation of the COSMO-SC turbulence scheme in a shear-driven stable boundary layer. *Meteor. Z.,* **20,** 335–350.

Christensen, J. H., T. R. Carter, M. Rummukainen, and G. Amanatidis, 2007: Evaluating the performance and utility of regional climate models: The PRUDENCE project. *Climatic Change,* **81,** 1–6.

Christensen, O. B., M. Drews, and J. H. Christensen, 2006: The HIRHAM regional climate model version 5. DMI Tech. Rep. 06-17, 22 pp.

Cook, K. H., and E. K. Vizy, 2006: Coupled model simulations of the West African monsoon system: Twentieth- and twenty-first-century simulations. *J. Climate,* **19,** 3681–3703.

Cuxart, J., P. Bougeault, and J.-L. Redelsperger, 2000: A turbulence scheme allowing for mesoscale and large-eddy simulations. *Quart. J. Roy. Meteor. Soc.,* **126,** 1–30.

Dai, A., 2001: Global precipitation and thunderstorm frequencies. Part II: Diurnal variations. *J. Climate,* **14,** 1112–1128.

——, and K. E. Trenberth, 2004: The diurnal cycle and its depiction in the Community Climate System Model. *J. Climate,* **17,** 930–951.

——, F. Giorgi, and K. E. Trenberth, 1999: Observed and model-simulated diurnal cycles over the contiguous United States. *J. Geophys. Res.,* **104** (D6), 6377–6402.

——, X. Lin, and K.-L. Hsu, 2007: The frequency, intensity, and diurnal cycle of precipitation in surface and satellite observations over low- and mid-latitudes. *Climate Dyn.,* **29,** 727–744.

da Rocha, R. P., C. A. Morales, S. V. Cuadra, and T. Ambrizzi, 2009: Precipitation diurnal cycle and summer climatology assessment over South America: An evaluation of Regional Climate Model version 3 simulations. *J. Geophys. Res.,* **114,** D10108, doi:10.1029/2008JD010212.

Dee, D. P., and Coauthors, 2011: The ERA-Interim reanalysis: Configuration and performance of the data assimilation system. *Quart. J. Roy. Meteor. Soc.,* **137,** 553–597.

Delage, Y., 1997: Parameterising sub-grid scale vertical transport in atmospheric models under statically stable conditions. *Bound.-Layer Meteor.,* **82,** 23–48.

Déqué, M., 2010: Regional climate simulation with a mosaic of RCMs. *Meteor. Z.,* **19,** 259–266.

Dickinson, R. E., A. Henderson-Sellers, and P. J. Kennedy, 1993: Biosphere-Atmosphere Transfer Scheme (BATS) version 1E as coupled to the NCAR Community Climate Model. NCAR Tech. Note NCAR/TN-387+STR, 72 pp.

Doms, G., and Coauthors, 2011: A description of the nonhydrostatic regional COSMO model. Part II: Physical parameterization. COSMO Rep. LM_F90 4.20, 154 pp. [Available online at http://www.cosmo-model.org/content/model/documentation/core/cosmoPhysParamtr.pdf.]

Douville, H. S., S. Planton, J.-F. Royer, D. B. Stephenson, S. Tyteca, L. Kergoat, S. Lafont, and R. A. Betts, 2000: Importance of vegetation feedbacks in doubled-CO_2 climate experiments. *J. Geophys. Res.,* **105** (D11), 14 841–14 861.

Druyan, L. M., and Coauthors, 2010: The WAMME regional model intercomparison study. *Climate Dyn.,* **35,** 175–192.

Dudhia, J., 1989: Numerical study of convection observed during the Winter Monsoon Experiment using a mesoscale two-dimensional model. *J. Atmos. Sci.,* **46,** 3077–3107.

ECMWF, 2007: IFS documentation—Cy31r1: Operational implementation 12 September 2006; Part IV: Physical processes. ECMWF Rep., 155 pp. [Available online at http://www.ecmwf.int/research/ifsdocs/CY31r1/PHYSICS/IFSPart4.pdf.]

Edwards, J. M., and A. Slingo, 1996: Studies with a flexible new radiation code. I: Choosing a configuration for a large-scale model. *Quart. J. Roy. Meteor. Soc.,* **122,** 689–719.

Essery, R. L. H., M. J. Best, R. A. Betts, and P. M. Cox, 2003: Explicit representation of subgrid heterogeneity in a GCM land surface scheme. *J. Hydrometeor.,* **4,** 530–543.

Fekete, B. M., C. J. Vörösmarty, J. O. Roads, and C. J. Willmott, 2004: Uncertainties in precipitation and their impacts on runoff estimates. *J. Climate,* **17,** 294–304.

Fouquart, Y., and B. Bonnel, 1980: Computations of solar heating of the earth's atmosphere: A new parameterization. *Beitr. Phys. Atmos.,* **53,** 35–62.

Fritsch, J. M., and C. F. Chappell, 1980: Numerical prediction of convectively driven mesoscale pressure systems. Part I: Convective parameterization. *J. Atmos. Sci.,* **37,** 1722–1733.

Giorgetta, M., and M. Wild, 1995: The water vapour continuum and its representation in ECHAM4. MPI Rep. 162, 38 pp.

Giorgi, F., C. Jones, and G. R. Asrar, 2009: Addressing climate information needs at the regional level: The CORDEX framework. *WMO Bull.,* **58,** 175–183.

Gregory, D., and P. R. Rowntree, 1990: A mass flux convection scheme with representation of cloud ensemble characteristics and stability-dependent closure. *Mon. Wea. Rev.,* **118,** 1483–1506.

——, and S. Allen, 1991: The effect of convective downdraughts upon NWP and climate simulations. Preprints, *Ninth Conf. on Numerical Weather Prediction,* Denver, CO, Amer. Meteor. Soc., 122–123.

Grell, G. A., 1993: Prognostic evaluation of assumptions used by cumulus parameterizations. *Mon. Wea. Rev.,* **121,** 764–787.

Gruber, A., X. Su, M. Kanamitsu, and J. Schemm, 2000: The comparison of two merged rain gauge–satellite precipitation datasets. *Bull. Amer. Meteor. Soc.,* **81,** 2631–2644.

Haensler, A., S. Hagemann, and D. Jacob, 2010: Dynamical downscaling of ERA40 reanalysis data over southern Africa:

Added value in the simulation of the seasonal rainfall characteristics. *Int. J. Climatol.,* **31,** 2338–2349, doi:10.1002/joc.2242.

Hagemann, S., 2002: An improved land surface parameter dataset for global and regional climate models. MPI Rep. 336, 21 pp.

Herzog, H.-J., G. Vogel, and U. Schubert, 2002: LLM—A nonhydrostatic model applied to high-resolving simulations of turbulent fluxes over heterogeneous terrain. *Theor. Appl. Climatol.,* **73,** 67–86.

Hodges, K. I., and C. D. Thorncroft, 1997: Distribution and statistics of African mesoscale convective weather systems based on the ISCCP Meteosat imagery. *Mon. Wea. Rev.,* **125,** 2821–2873.

Holtslag, A. A. M., E. I. F. de Bruijn, and H.-L. Pan, 1990: A high resolution air mass transformation model for short-range weather forecasting. *Mon. Wea. Rev.,* **118,** 1561–1575.

Hong, S.-Y., J. Dudhia, and S.-H. Chen, 2004: A revised approach to ice microphysical processes for the bulk parameterization of clouds and precipitation. *Mon. Wea. Rev.,* **132,** 103–120.

——, Y. Noh, and J. Dudhia, 2006: A new vertical diffusion package with an explicit treatment of entrainment processes. *Mon. Wea. Rev.,* **134,** 2318–2341.

Huffman, G. J., and D. T. Bolvin, 2011: TRMM and other data precipitation data set documentation. NASA GSFC Rep., 29 pp. [Available online at ftp://precip.gsfc.nasa.gov/pub/trmmdocs/3B42_3B43_doc.pdf.]

——, R. F. Adler, M. M. Morrissey, D. T. Bolvin, S. Curtis, R. Joyce, B. McGavock, and J. Susskind, 2001: Global precipitation at one-degree daily resolution from multisatellite observations. *J. Hydrometeor.,* **2,** 36–50.

——, and Coauthors, 2007: The TRMM Multisatellite Precipitation Analysis (TMPA): Quasi-global, multiyear, combined-sensor precipitation estimates at fine scales. *J. Hydrometeor.,* **8,** 38–55.

——, R. F. Adler, D. T. Bolvin, and G. Gu, 2009: Improving the global precipitation record: GPCP version 2.1. *Geophys. Res. Lett.,* **36,** L17808, doi:10.1029/2009GL040000.

Jacob, D., 2001: A note to the simulation of the annual and interannual variability of the water budget over the Baltic Sea drainage basin. *Meteor. Atmos. Phys.,* **77,** 61–73.

——, and Coauthors, 2007: An inter-comparison of regional climate models for Europe: Design of the experiments and model performance. *Climatic Change,* **81,** 31–52.

Janicot, S., 2009: A comparison of Indian and African monsoon variability at different time scales. *C. R. Geosci.,* **341,** 575–590.

Jeong, J.-H., A. Walther, G. Nikulin, D. Chen, and C. Jones, 2011: Diurnal cycle of precipitation amount and frequency in Sweden: Observation versus model simulation. *Tellus,* **63A,** 664–674, doi:10.1111/j.1600-0870.2011.00517.x.

Jones, C. G., F. Giorgi, and G. Asrar, 2011: The Coordinated Regional Downscaling Experiment: CORDEX; An international downscaling link to CMIP5. *CLIVAR Exchanges,* International CLIVAR Project Office, No. 56, Southampton, United Kingdom, 34–40. [Available online at http://www.clivar.org/sites/default/files/imported/publications/exchanges/Exchanges_56.pdf.]

Jones, P. W., 1999: First- and second-order conservative remapping schemes for grids in spherical coordinates. *Mon. Wea. Rev.,* **127,** 2204–2210.

Jones, R. G., M. Noguer, D. Hassel, D. Hudson, S. Wilson, G. Jenkins, and J. Mitchell, 2004: Generating high resolution climate change scenarios using PRECIS. Met Office Hadley Centre Handbook, 40 pp. [Available online at http://www.metoffice.gov.uk/media/pdf/6/5/PRECIS_Handbook.pdf.]

Joyce, R. J., J. E. Janowiak, P. A. Arkin, and P. Xie, 2004: CMORPH: A method that produces global precipitation estimates from passive microwave and infrared data at high spatial and temporal resolution. *J. Hydrometeor.,* **5,** 487–503.

Kain, J. S., 2004: The Kain–Fritsch convective parameterization: An update. *J. Appl. Meteor.,* **43,** 170–181.

——, and J. M. Fritsch, 1990: A one-dimensional entraining/detraining plume model and its application in convective parameterization. *J. Atmos. Sci.,* **47,** 2784–2802.

——, and ——, 1993: Convective parameterization for mesoscale models: The Kain-Fritsch scheme. *The Representation of Cumulus Convection in Numerical Models, Meteor. Monogr.,* No. 46, Amer. Meteor. Soc., 165–170.

Kiehl, J. T., J. J. Hack, G. B. Bonan, B. A. Boville, B. P. Briegleb, D. L. Williamson, and P. J. Rasch, 1996: Description of the NCAR Community Climate Model (CCM3). NCAR Tech. Note NCAR/TN-420+STR, 152 pp.

Kikuchi, K., and B. Wang, 2008: Diurnal precipitation regimes in the global tropics. *J. Climate,* **21,** 2680–2696.

Kuo, H. L., 1965: On formation and intensification of tropical cyclones through latent heat release by cumulus convection. *J. Atmos. Sci.,* **22,** 40–63.

Legates, D. R., and C. J. Willmott, 1990: Mean seasonal and spatial variability in gauge-corrected, global precipitation. *Int. J. Climatol.,* **10,** 111–127.

Li, J., and H. W. Barker, 2005: A radiation algorithm with correlated-*k* distribution. Part I: Local thermal equilibrium. *J. Atmos. Sci.,* **62,** 286–309.

Liang, X.-Z., L. Li, A. Dai, and K. E. Kunkel, 2004: Regional climate model simulation of summer precipitation diurnal cycle over the United States. *Geophys. Res. Lett.,* **31,** L24208, doi:10.1029/2004GL021054.

Lohmann, U., and E. Roeckner, 1996: Design and performance of a new cloud microphysics scheme developed for the ECHAM general circulation model. *Climate Dyn.,* **12,** 557–572.

Louis, J. F., 1979: A parametric model of vertical eddy fluxes in the atmosphere. *Bound.-Layer Meteor.,* **17,** 187–202.

Lynn, B. H., R. Healy, and L. M. Druyan, 2007: An analysis of the potential for extreme temperature change based on observations and model simulations. *J. Climate,* **20,** 1539–1554.

McGarry, M. M., and R. J. Reed, 1978: Diurnal variations in convective activity and precipitation during phases II and III of GATE. *Mon. Wea. Rev.,* **106,** 101–113.

Mearns, L. O., W. Gutowski, R. Jones, R. Leung, S. McGinnis, A. Nunes, and Y. Qian, 2009: A regional climate change assessment program for North America. *Eos, Trans. Amer. Geophys. Union,* **90,** doi:10.1029/2009EO360002.

Mellor, G. L., and T. Yamada, 1982: Development of a turbulence closure model for geophysical fluid problems. *Rev. Geophys. Space Phys.,* **20,** 851–875.

Menéndez, C. G., M. de Castro, A. Sorensson, and J.-P. Boulanger, 2010: CLARIS project: Towards climate downscaling in South America. *Meteor. Z.,* **19,** 357–362.

Mitchell, T. D., and P. D. Jones, 2005: An improved method of constructing a database of monthly climate observations and associated high-resolution grids. *Int. J. Climatol.,* **25,** 693–712, doi:10.1002/joc.1181.

Mlawer, E. J., S. J. Taubman, P. D. Brown, M. J. Iacono, and S. A. Clough, 1997: Radiative transfer for inhomogeneous atmospheres: RRTM, a validated correlated-k model for the longwave. *J. Geophys. Res.,* **102** (D14), 16 663–16 682.

Morcrette, J.-J., 1990: Impact of changes to the radiation transfer parameterizations plus cloud optical properties in the ECMWF model. *Mon. Wea. Rev.,* **118,** 847–873.

——, L. Smith, and Y. Fouquart, 1986: Pressure and temperature dependence of the absorption in longwave radiation parametrizations. *Beitr. Phys. Atmos.,* **59,** 455–469.

Oouchi, K., J. Yoshimura, H. Yoshimura, R. Mizuta, S. Kusunoki, and A. Noda, 2006: Tropical cyclone climatology in a global-warming climate as simulated in a 20 km-mesh global tmospheric model: Frequency and wind intensity analyses. *J. Meteor. Soc. Japan,* **84,** 259–276.

Paeth, H., K. Born, R. Podzun, and D. Jacob, 2005: Regional dynamical downscaling over West Africa: Model evaluation and comparison of wet and dry years. *Meteor. Z.,* **14,** 349–367.

——, and Coauthors, 2011: Progress in regional downscaling of West African precipitation. *Atmos. Sci. Lett.,* **12,** 75–82.

Pal, J. S., E. E. Small, and E. A. B. Eltahir, 2000: Simulation of regional-scale water and energy budgets: Representation of subgrid cloud and precipitation processes within RegCM. *J. Geophys. Res.,* **105** (D24), 29 579–29 594.

——, and Coauthors, 2007: Regional climate modeling for the developing world: The ICTP RegCM3 and RegCNET. *Bull. Amer. Meteor. Soc.,* **88,** 1395–1409.

Patricola, C. M., and C. H. Cook, 2010: Northern African climate at the end of the twenty-first century: An integrated application of regional and global climate models. *Climate Dyn.,* **35,** 193–212.

Pinker, R. T., Y. Zhao, C. Akoshile, J. Janowiak, and P. Arkin, 2006: Diurnal and seasonal variability of rainfall in the sub-Sahel as seen from observations, satellites and a numerical model. *Geophys. Res. Lett.,* **33,** L07806, doi:10.1029/2005GL025192.

Rasch, P. J., and J. E. Kristjánsson, 1998: A comparison of the CCM3 model climate using diagnosed and predicted condensate parameterizations. *J. Climate,* **11,** 1587–1614.

Ratnam, J. V., F. Giorgi, A. Kaginalkar, and S. Cozzini, 2009: Simulation of the Indian monsoon using the RegCM3-ROMS regional coupled model. *Climate Dyn.,* **33,** 119–139.

Rechid, D., T. J. Raddatz, and D. Jacob, 2009: Parameterization of snow-free land surface albedo as a function of vegetation phenology based on MODIS data and applied in climate modelling. *Theor. Appl. Climatol.,* **95,** 245–255.

Ricard, J. L., and J. F. Royer, 1993: A statistical cloud scheme for use in an AGCM. *Ann. Geophys.,* **11,** 1095–1115.

Ritter, B., and J.-F. Geleyn, 1992: A comprehensive radiation scheme of numerical weather prediction with potential application to climate simulations. *Mon. Wea. Rev.,* **120,** 303–325.

Rockel, B., A. Will, and A. Hense, 2008: The regional climate model COSMO-CLM (CCLM). *Meteor. Z.,* **17,** 347–248.

Rudolf, B., A. Becker, U. Schneider, A. Meyer-Christoffer, and M. Ziese, 2010: The new ''GPCC full data reanalysis version 5'' providing high-quality gridded monthly precipitation data for the global land-surface is public available since December 2010. GPCC Status Rep., 7 pp.

Ruti, P. M., and Coauthors, 2011: The West African climate system: A review of the AMMA model inter-comparison initiatives. *Atmos. Sci. Lett.,* **12,** 116–122.

Samuelsson, P., S. Gollvik, and A. Ullerstig, 2006: The land-surface scheme of the Rossby Centre regional atmospheric climate model (RCA3). SMHI Rep. Met. 122, 25 pp.

——, and Coauthors, 2011: The Rossby Centre regional climate model RCA3: Model description and performance. *Tellus,* **63A,** 4–23.

Sass, B. H., L. Rontu, H. Savijärvi, and P. Räisänen, 1994: HIRLAM-2 radiation scheme: Documentation and tests. SMHI HIRLAM Tech. Rep. 16, 43 pp.

Savijärvi, H., 1990: A fast radiation scheme for mesoscale model and short-range forecast models. *J. Appl. Meteor.,* **29,** 437–447.

Schulz, J.-P., L. Dümenil, J. Polcher, C. A. Schlosser, and Y. Xue, 1998: Land surface energy and moisture fluxes: Comparing three models. *J. Appl. Meteor.,* **37,** 288–307.

Shin, D. W., S. Cocke, and T. E. LaRow, 2007: Diurnal cycle of precipitation in a climate model. *J. Geophys. Res.,* **112,** D13109, doi:10.1029/2006JD008333.

Skamarock, W. C., J. B. Klemp, J. Dudhia, D. O. Gill, D. M. Barker, W. Wang, and J. G. Powers, 2008: A description of the advanced research WRF version 3. NCAR Tech. Note NCAR/TN-475+STR, 113 pp.

Smirnova, T. G., J. M. Brown, S. G. Benjamin, and D. Kim, 2000: Parameterization of cold-season processes in the MAPS land-surface scheme. *J. Geophys. Res.,* **105** (D3), 4077–4086.

Smith, R. N. B., 1990: A scheme for predicting layer clouds and their water content in a general circulation model. *Quart. J. Roy. Meteor. Soc.,* **116,** 435–460.

Smith, S. W., 2002: *Digital Signal Processing: A Practical Guide for Engineers and Scientists*. Newnes, 672 pp.

Sultan, B., and S. Janicot, 2000: Abrupt shift of the ITCZ over West Africa and intra-seasonal variability. *Geophys. Res. Lett.,* **27,** 3353–3356.

Sundqvist, H., E. Berge, and J. E. Kristjansson, 1989: Condensation and cloud parameterization studies with a mesoscale numerical weather prediction model. *Mon. Wea. Rev.,* **117,** 1641–1657.

Sylla, M. B., A. T. Gaye, J. S. Pal, G. S. Jenkins, and X. Q. Bi, 2009: High-resolution simulations of West African climate using regional climate model (RegCM3) with different lateral boundary conditions. *Theor. Appl. Climatol.,* **98,** 293–314.

——, E. Coppola, L. Mariotti, F. Giorgi, P. M. Ruti, A. Dell'Aquila, and X. Bi, 2010: Multiyear simulation of the African climate using a regional climate model (RegCM3) with the high resolution ERA-Interim reanalysis. *Climate Dyn.,* **35,** 231–247.

Tadross, M. A., W. J. Gutowski Jr., B. C. Hewitson, C. Jack, and M. New, 2006: MM5 simulations of interannual change and the diurnal cycle of southern African regional climate. *Theor. Appl. Climatol.,* **86,** 63–80.

Tiedtke, M., 1989: A comprehensive mass flux scheme for cumulus parameterization in large-scale models. *Mon. Wea. Rev.,* **117,** 1779–1800.

——, 1993: Representation of clouds in large-scale models. *Mon. Wea. Rev.,* **121,** 3040–3061.

Tompkins, A. M., 2002: A prognostic parameterization for the subgrid-scale variability of water vapor and clouds in large-scale models and its use to diagnose cloud cover. *J. Atmos. Sci.,* **59,** 1917–1942.

van der Linden, P., and J. F. B. Mitchell, Eds., 2009: ENSEMBLES: Climate change and its impacts at seasonal, decadal and centennial timescales; Summary of research and results from the ENSEMBLES project. Met Office Hadley Centre Rep., 160 pp.

van Meijgaard, E., L. H. van Ulft, W. J. van den Berg, F. C. Bosveld, B. J. J. M. van den Hurk, G. Lenderink, and A. P. Siebesma, 2008: The KNMI regional atmospheric climate model RACMO version 2.1. KNMI Tech. Rep. TR-302, 43 pp.

Verseghy, D. L., 2000: The Canadian Land Surface Scheme (CLASS): Its history and future. *Atmos.–Ocean,* **38,** 1–13.

von Storch, H., H. Langenberg, and F. Feser, 2000: A spectral nudging technique for dynamical downscaling purposes. *Mon. Wea. Rev.,* **128,** 3664–3673.

Wilson, C. A., 1992: Vertical diffusion. NWP Meteorological Office Unified Model Documentation Paper 21, version 4.0, 4 pp.

Xi, P., B. Rudolf, U. Schneider, and P. A. Arkin, 1996: Gauge-based monthly analysis of global land precipitation from 1971 to 1994. *J. Geophys. Res.,* **101** (D14), 19 023–19 034.

Xue, Y., and Coauthors, 2010: Intercomparison and analyses of the climatology of the West African monsoon in the West African Monsoon Modeling and Evaluation Project (WAMME) first model intercomparison experiment. *Climate Dyn.,* **35,** 3–27.

Yamamoto, M. K., F. A. Furuzawa, A. Higuchi, and K. Nakamura, 2008: Comparison of diurnal variations in precipitation systems observed by TRMM PR, TMI, and VIRS. *J. Climate,* **21,** 4011–4028.

Yang, S., and J. Slingo, 2001: The diurnal cycle in the tropics. *Mon. Wea. Rev.,* **129,** 784–801.

——, and E. A. Smith, 2006: Mechanisms for diurnal variability of global tropical rainfall observed from TRMM. *J. Climate,* **19,** 5190–5226.

Yin, X., and A. Gruber, 2010: Validation of the abrupt change in GPCP precipitation in the Congo River basin. *Int. J. Climatol.,* **30,** 110–119.

Zadra, A., D. Caya, J. Côté, B. Dugas, C. Jones, R. Laprise, K. Winger, and L.-P. Caron, 2008: The next Canadian Regional Climate Model. *Phys. Canada,* **64,** 75–83.